Study and quantification of enantiodiscrimination power of four polymeric chiral LLCs using NAD 2D-NMR

Philippe Berdagué [a], Boris Gouilleux, [a], Markus Noll[b], Stefan Immel [b], Michael Reggelin *, [b] and Philippe Lesot *, [a, c]

[a] Université Paris-Saclay, UFR d'Orsay, RMN en Milieu Orienté, ICMMO, UMR CNRS 8182, Bât. 410, F-91405 Orsay cedex, France.
[b] Clemens-Schöpf-Institut für Organische Chemie und Biochemie Technische Universität Darmstadt Alarich-Weiss-Strasse 4, 64287 Darmstadt, Germany.
[c] Centre National de la Recherche Scientifique (CNRS), 3 rue Michel Ange, F-75016 Paris, France.

Mail: philippe.lesot@universite-paris-saclay.fr
Mail: re@chemie.tu-darmstadt.de

Index of the Electronic Supporting Information

I. Qualitative analysis of a series of chiral secondary alcohols in PLA and PBLG mesophases

In a recent work, we have qualitatively examined the enantiodiscriminating abilities of a polyacetylene-based chiral polymer (PLA) compared with the historical polypeptide-based polymer (PBLG), by screening a large collection of mono- (or per-) deuterated chiral analytes [**1**].

From ^{2}H NMR, it is possible to compare a series of "homologous/similar" chiral compounds dissolved in two mesophases at the same temperature, by analyzing: i) the magnitude of the average of residual quadrupolar coupling noted ^{2}H-RQC^{aver}, defined $|\Delta\nu_Q^{aver}(^2H)| = [|\Delta\nu_Q^R(^2H)| + |\Delta\nu_Q^S(^2H)|]/2)$ that is related to the degree of orientation of a given C-D bond, and ii) the difference of ^{2}H-RQCs ($|\Delta\Delta\nu_Q(^2H)| = \left|\left|\Delta\nu_{Q_i}^S\right| - \left|\Delta\nu_{Q_i}^R\right|\right|$ that can be regarded as the spectral enantiodiscrimination magnitude. Examples of comparative charts based on quantities $|\Delta\nu_Q^{aver}(^2H)|$ and $|\Delta\Delta\nu_Q|$ are given in **Figures SI-1** and **SI-2** exemplified by a series of six chiral secondary alcohols deuterated on the stereogenic center (R_1-C*D(OH)-R_2) oriented in the PLA/$CHCl_3$ and PBLG/$CHCl_3$ mesophase. Numerical data can be found in **Ref.** [**1**]. The series of analytes is sorted out on the basis of three molecular criteria (molecular specificities): i) the molecular shape anisotropy and in particular difference of the persistent volume of the R_1 and R_2 substituents (V_{R1} and V_{R2}); ii) the polarity of the R_1 and R_2 substituents; and iii) the position (central or terminal) of the OH group that is likely to form an H bond with the polymer side chains).

A simple evaluation of EDAs at a given deuterated site can be achieved by determining the local "differential ordering effect" (DOE factor) calculated as $\Delta\Delta\nu_Q(^2H)$ over their mean values [**2**]:

$$\mathrm{DOE}\left(^2\mathrm{H}\right)_i = 2 \times \frac{\left|\left|\Delta\nu_{Q_i}^S\right| - \left|\Delta\nu_{Q_i}^R\right|\right|}{\left|\Delta\nu_{Q_i}^S\right| + \left|\Delta\nu_{Q_i}^R\right|}. \qquad \textbf{(S-1)}$$

This DOE factor can be considered as a local quantification factor of the orientational deviation for a given site in the *R/S* isomers with the situation that would be observed in an achiral mesophase where no discrimination is possible [**3**].

Figure SI-3 presents the comparison of DOE factors on the same series of analytes mentioned above interacting with two chiral phases. On this comparative graph, the analytes of the series are sorted according to three criteria: i) the molecular shape anisotropy regarding the difference of the persistent volume of the R_1 and R_2 substituents (V_{R1} and V_{R2}); ii) the polarity of R_1 and R_2 moieties, and iii) the position (central or terminal) of the OH group that is likely to form an H bond with both polymers [**4**].

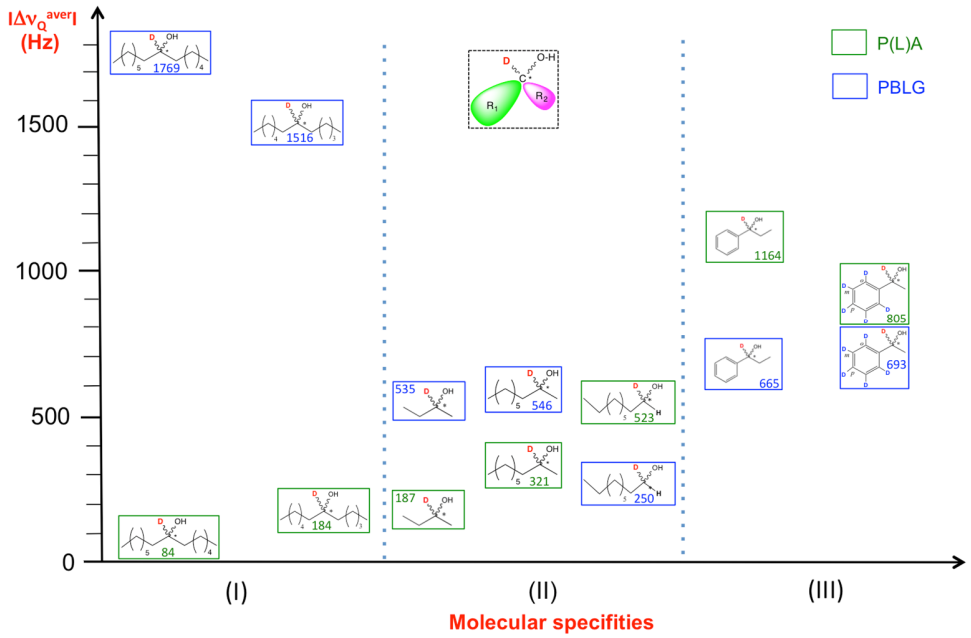

Figure SI-1. Intercomparison of $|\Delta\nu_Q^{aver}|$ values (absolute values) of a series of monodeuterated secondary chiral alcohols measured in PLA/$CHCl_3$ and PBLG/$CHCl_3$ mesophases (green and blue frame) at 300 K. Molecular specificities of these series of monostereogenic chiral alcohols are sorted out in three groups (see text). Data are extracted from **Ref.** [**1**].

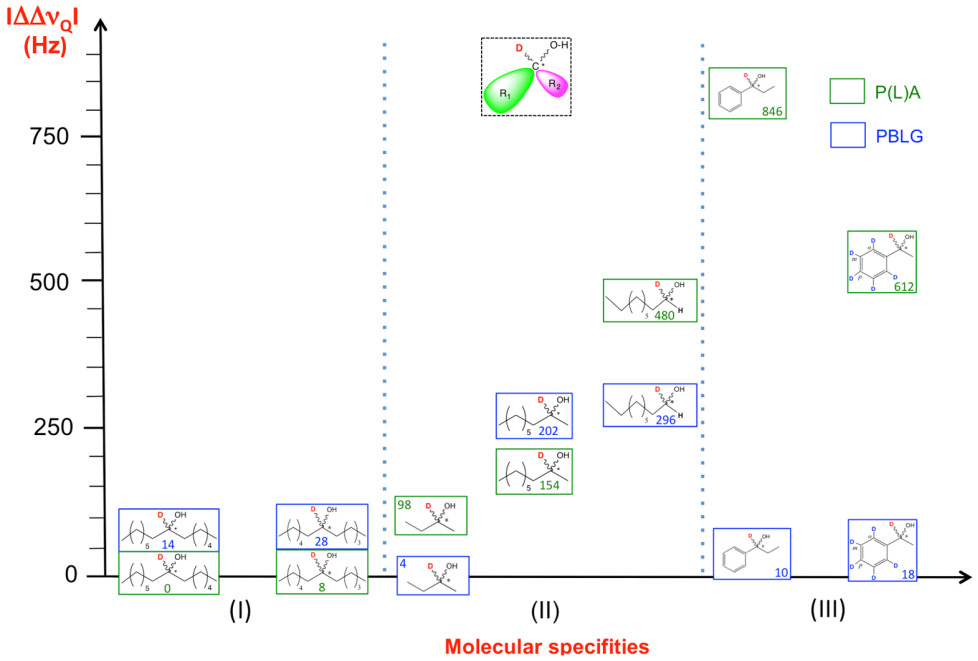

Figure SI-2. Intercomparison of $|\Delta\Delta\nu_Q|$ values (absolute values) of a series of simple, monodeuterated secondary chiral alcohols measured in PLA/$CHCl_3$ and PBLG/$CHCl_3$ mesophases (green and blue frame) at 300 K. Molecular specificities of these series of monostereogenic chiral alcohols are sorted out in three groups (see text). Data are extracted from **Ref.** [**1**].

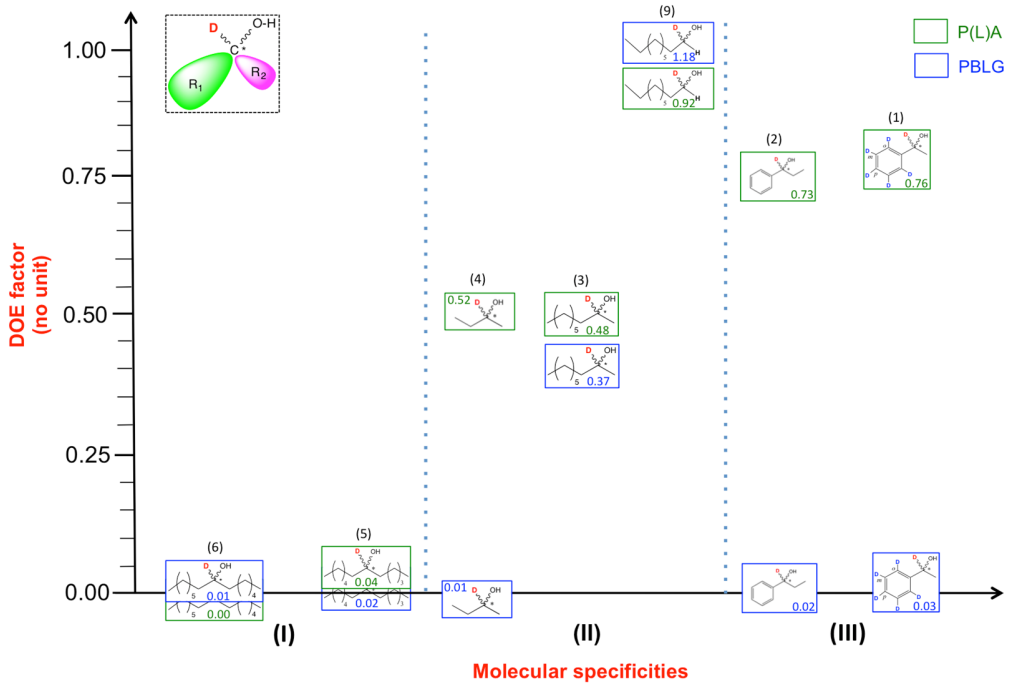

Figure SI-3. Intercomparison of DOE(^{2}H) factors of a series of simple, monodeuterated secondary chiral alcohols measured in PLA/$CHCl_3$ and PBLG/$CHCl_3$ mesophases (green and blue frame, respectively) at 300 K. Molecular specificities of this series of chiral alcohols are sorted out in three groups (see text). Comparative graph constructed from experimental data extracted from **Ref.** [**1**].

A first analysis of results in PLA indicates that higher DOE factors are obtained when the $V_{R1} >> V_{R2}$ with a bonus when an electron-enriched moiety (aromatic) is included (analytes 1, 2 of group III). In contrast, molecules having similar R_1, R_2 volumes and rather weakly polar, flexible group (alkyl) (analytes **5**, **6** of group I) are the most weakly enantiodiscriminated, and suggesting the importance of shape anisotropy around the stereogenic center in the efficiency of CDM. In case of **6**, for instance, the small difference between V_{R1} and V_{R2} ($V_{R1} \approx V_{R2}$) can also explain DOE values close to zero, because, from a Van der Waals volume point of view, alcohol **6** appears to be more of C_{2V}-symmetry (than C_1-symmetry), for which no spectral enantiodiscrimination is expected in the plane of symmetry (the C*-D direction) [**4, 5**].

Finally, with the exception of analyte **9** which is chiral by virtue of the (^{2}H/^{1}H) isotopic substitution, structures characterised by $V_{R1} > V_{R2}$ but not by a polar R_1/R_2 substituent (analytes **3**, **4** of group II) exhibit intermediate DOEs, while larger DOEs were obtained with PLA phase compared to PBLG. Actually, although chiral with a C_1-symmetry, the enantiomeric discrimination obtained at the stereogenic center for **9** is the consequence of the enantiotopic discrimination that would be observed with the parent prochiral molecule (R-CD_2-OH) of C_s-symmetry [**6**]. In terms of molecular electronic topology, alcohol **9** should be more considered as a prochiral object of C_s-symmetry rather than a chiral one of C_1-symmetry) [**4, 6**].

Although useful, the comparison and the interpretation of such result in terms of electronic properties and/or topological profile (shape anisotropy) of chiral analytes is probably perilous for a robust phenomenological description of CDMs because a single C-D internuclear direction is probed.

II. From ^{2}H-RQC data to the Saupe order matrix

This principle of the ^{2}H-RQC-based ConArch$^{+\,+}$ program relies on the idea that there is a unique relationship (**Eq. S-2**) linking the set of experimental, $\Delta\nu_{Qi}^{Exptl.}$, the Saupe order matrix, $\{S_{\alpha\beta}\}$, expressed in an axis system (α, β = a, b, c) attached to the molecule (description of the molecule orientation) and the geometry (3D structure) of the molecule obtained by molecular modeling (DFT calculation) [**7, 8**]:

$$\frac{2}{3}\times\frac{\Delta\nu_{Q_i}^{Expt.}}{K_{D_i}} = \sum_{\alpha\beta=a,b,c}\cos\theta_{\alpha_{C-D_i}}\cos\theta_{\beta_{C-D_i}}S_{\alpha\beta} \qquad \textbf{(S-2)}$$

where K_{D_i} corresponds to the quadrupolar coupling constant associated with a site i. Thus, the ConArch$^+$ program will vary the Saupe order parameters, $S_{\alpha\beta}$, (via an algorithm based on the principle of singular value decomposition (SVD)) in order to minimize the difference between the experimental values, $\Delta\nu_Q^{Exptl.}$, and the back-calculated values of $\Delta\nu_Q^{Calc.}$, from the order matrix for a given geometry [**9**]. The principle of the determination of ^{2}H-RQCs (with sign) and the ConArch$^+$ program is schematically presented in **Figure SI-5**.

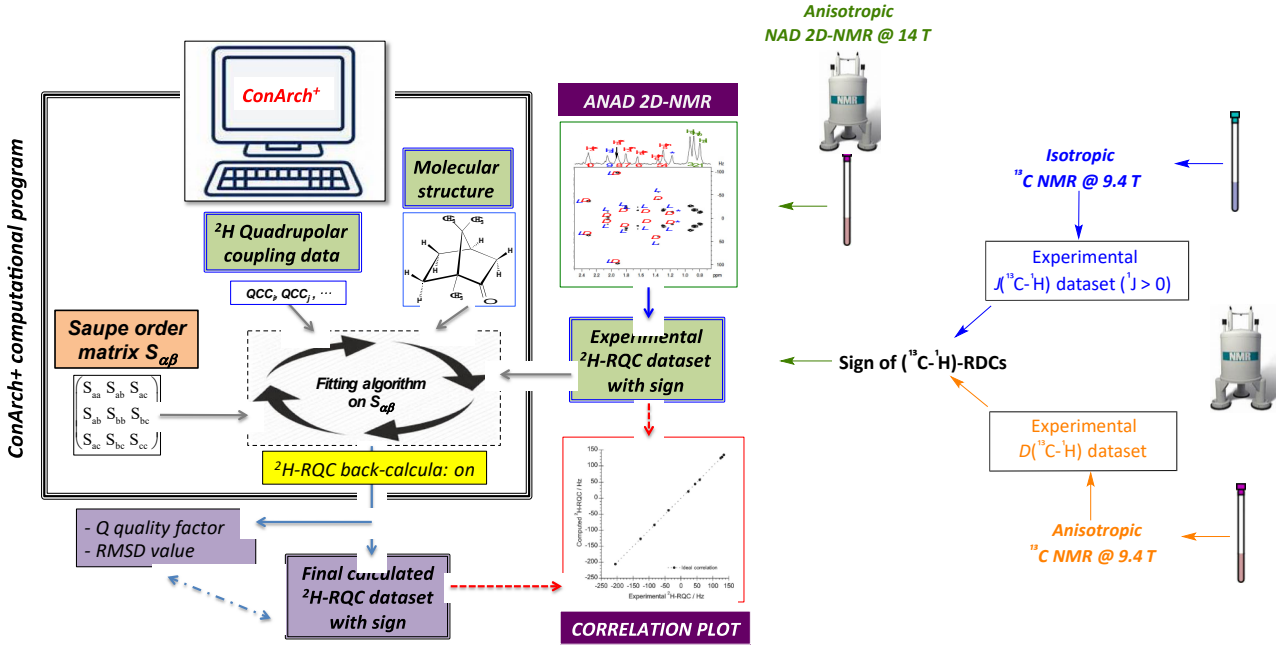

Figure SI-4. Schematic description of the operating principle of ConArch$^+$ program using ^{2}H-RQC dataset as input. In contrast to tools using RDC data, only the sign of ^{1}D(^{13}C-^{1}H) couplings needs to be known. Since an exact measurement of $^1D(^{13}C\text{-}^1H)$ values is not necessary, the implementation of sophisticated ^{13}C-^{1}H heteronuclear 2D experiments is not (always) necessary.

The quality of agreement between $\Delta\nu_Q^{Exptl.}$ and $\Delta\nu_Q^{Calc.}$ is numerically evaluated using the Cornilescu's quality factor, Q, calculated as follows [**10**]:

$$Q = \sqrt{\frac{\sum w_n\left(\Delta\nu_Q^{Exptl.}(^2\mathrm{H}) - \Delta\nu_Q^{Calc.}(^2\mathrm{H})\right)^2}{\sum w_n\left(\Delta\nu_Q^{Exptl.}(^2\mathrm{H})\right)^2}} \qquad \textbf{(S-3)}$$

where w_n are normalized relative weighting factors. For uniform weighting, w_n is equal to one for all ^{2}H-RQC used.

In practice, the smaller the value of Q, the better the agreement. The quality of fit can also be evaluated by calculating the standard deviation of residues from **Eq. S-4**. As for Q value, the smaller the value of the RMSD, the better the matching.

$$RMSD = \sqrt{\frac{1}{N}\sum\left(\Delta\nu_Q^{Exptl.}(^2\mathrm{H}) - \Delta\nu_Q^{Calc.}(^2\mathrm{H})\right)^2} \qquad \textbf{(S-4)}$$

where N corresponds to the number of ^{2}H-RQC considered. Finally, the quality of the agreement between $\Delta\nu_Q^{Exptl.}$ and $\Delta\nu_Q^{Calc.}$ can be simply presented graphically with the help of a correlation plot ($\Delta\nu_Q^{Exptl.}$ *versus* $\Delta\nu_Q^{Calc.}$) as depicted in **Figure SI-4**.

From the elements, $S_{x'x}$, $S_{y'y}$ and $S_{z'z'}$ of the diagonalized Saupe matrix describing the orientational behavior, several key tensorial properties can be calculated [**12**]. The most important parameters for the present study, the intertensor angle β and its cosine the GCB have been described in the main text. Another important parameter is the generalized degree of order (GDO), which is calculated as follows.

The generalized degree of order: The concept of generalized degree of order (GDO) in the principal axis system has been introduced to describe the orientational order of an analyte using a single value (scalar quantity). From the alignment tensor, $\boldsymbol{A}$, the value of GDO is defined as follows [**11, 12**]:

$$\mathrm{GDO} = \frac{|\boldsymbol{A}|}{|\mathbf{A}_{\max}|} = \sqrt{\frac{3}{2}}|\boldsymbol{A}| \qquad \textbf{(S-5)}$$

where $|\boldsymbol{A}|$ is the norm of the alignment tensor, $\boldsymbol{A}$, and $|\boldsymbol{A}_{\max}|$ represents the maximum order for a static molecule (solid state). Note here that the relation between the order matrix, noted, $\boldsymbol{S}$, and the alignment

tensor, noted $\boldsymbol{A}$, is simply defined as $\boldsymbol{A} = \frac{2}{3}\boldsymbol{S}$ [**12**]. Since in the principal axis system (x', y', z'), only the diagonal elements of $\boldsymbol{A}$ are non-zero, the above equation is reduced to:

$$\mathrm{GDO} = \sqrt{\frac{3}{2}}\sqrt{\left|A^2_{x'x'} + A^2_{y'y'} + A^2_{z'z'}\right|} \qquad \textbf{(S-6)}$$

Interestingly, the GDO values can be correlated depending on the size and shape of the molecule.

III.1 Preparation of 1 and *poly*-1 (*L*-MSP)

III.1 Materials and instrumentation

Solvents and reagents: Dichloromethane (DCM), chloroform [D_1] ($CDCl_3$) and triethylamine (Et_3N) were distilled from CaH_2 under argon atmosphere. Tetrahydrofuran (THF) was distilled from sodium-benzophenone under argon. Reagents were obtained from commercial sources and used without further purification unless otherwise specified. Moisture and/or air sensitive experiments were conducted under argon atmosphere using typical Schlenk techniques.

Thin layer chromatography (TLC): Thin-layer chromatography (TLC) was performed using E. Merck silica gel SilG/UV254 by Macherey Nagel & Co., Düren (thickness of layer 0.2 mm) and visualized by UV fluorescence quenching, oxidizing with $KMnO_4$ or ninhydrine stain.

Melting points were determined with the apparatus SG2000 manufactured by HWS Laboratoriumstechnik Mainz.

NMR-Spectra: ^{1}H-NMR spectra were recorded on Bruker ARX 300 and DRX 500 spectrometers operating at 300 and 500 MHz, respectively at 300 K unless otherwise specified. ^{13}C-NMR spectra were recorded on the same instruments at 75 and 125 MHz, respectively. Chemical shifts (δ) in ^{1}H-NMR and ^{13}C-NMR spectra are reported in ppm. The spectra were referenced against the residual solvent signal as reported in the literature [**13**]. The fine structure of proton signals was specified as s (singlet), d (doublet), t (triplet), q (quartet), m (multiplet), dd (doublet of doublet), br (broad).

IR-spectra were recorded on a Perkin-Elmer spectrometer Paragon 1000 PC or on a Vector 22 spectrometer from Bruker.

Gel permeation chromatography (GPC): Gel permeation chromatography was performed on two columns (MZ-Gel Sdplus 10^3 Å and 10^5 Å from MZ-Analysentechnik) in an oven at 30°C at a flow rate of 1.0 mL/min and pressure of 35-38 bar (HPLC pump from JASCO). The detector employed was a JASCO UV975-detector operating at 254 nm. Calibration was done using polystyrene standards from

Macherey-Nagel GmbH & Co. KG. The chromatograms were analysed using the software package WinGPC from Polymer Standard Service GmbH, Mainz (Germany). Typically about 3 mg of the polymer were dissolved in THF (containing one drop of toluene per 10 mL of solvent as internal standard; eluting after 25 minutes). 50µL of this solution were injected, the eluent was THF.

Sample centrifugation: Centrifugation was performed on a Rotina 46 (Fa. Hettich).

Specific optical rotations were determined on a Perkin Elmer Polarimeter 241 with Haake D8 thermostat or on an Anton Paar MCP 300 polarimeter in 1 dm cuvettes respectively.

CD spectra were recorded on a JASCO J-810 spectrometer equipped with a PTC-423S/15 Peltier element as a temperature device.

III.2 Monomer synthesis

III.2.1 *L*-Serine decyl ester hydrotosylate (9)

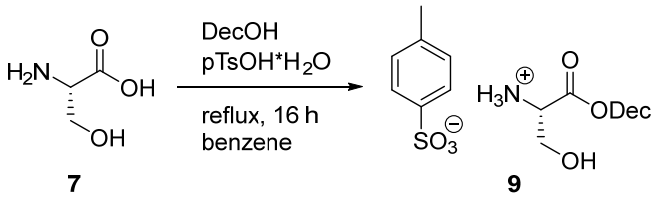

7 **9**

Inspired by the literature [**14**] a suspension of *L*-serine **7** (14.0 g, 133.2 mmol, 1.0 eq.), 1-decanol (50.8 mL, 42.2 g, 266.4 mmol, 2.0 eq.) and *p*-toluenesulfonic acid monohydrate (30.4 g, 159.9 mmol, 1.2 eq.) in 150 mL of benzene was refluxed for 16 h in a Dean-Stark water trap. About 100 mL of benzene were distilled off from the obtained solution under reduced pressure and the residue was poured into 350 mL of petroleum ether under vigorous stirring. The resulting solution was stored at -20°C overnight to produce a colorless precipitate. The solid was separated by filtration, washed thoroughly with petroleum ether and dried *in vacuo* to give 46.84 g (112.2 mmol) of **9**. Yield 84 %.

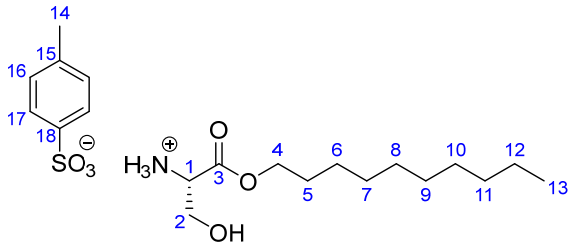

9

T_m = 85°C

^{1}H-NMR: ($CDCl_3$, 300 MHz, 300 K): δ = 8.03 (bd, 3H, ^{3}J = 4.4 Hz, NH_3), 7.73 (d, 2H, ^{3}J = 8.2 Hz, 17-H), 7.12 (d, 2H, ^{3}J = 8.2 Hz, 16-H), 4.25 (bs, 1H, OH), 4.13-3.95 (m, 4H, 1,2b,4-H), 3.88 (dd, 1H, ^{2}J = 12.4 Hz, ^{3}J = 4.6 Hz, 2a-H), 2.34 (s, 3H, 14-H), 1.50 („quint“, 2H, 5-H), 1.35–1.13 (m, 14H, 6,7,8,9,10,11,12-H), 0.88 (t, 3H, ^{3}J = 6.7 Hz, 13-H) ppm.

^{13}C-NMR: ($CDCl_3$, 125 MHz, 300 K): δ = 167.9 (3-C), 141.2 1 (18-C), 140.6 (15-C), 129.0 (16-C), 126.1 (17-C), 66.8 (4-C), 60.0 (2-C), 55.5 (1-C), 31.9 (11-C), 29.6 + 29.6 + 29.4 (8,9,10-C), 29.3 (7-C), 28.3 (5-C), 25.7 (6-C), 22.7 (12-C), 21.4 (14-C), 14.1 (13-C) ppm.

IR (KBr)**:** $\tilde{\nu}$ = 3040 (-NH_3^+), 2919 (-CH_2), 2856 (-CH_2), 1738 (COOR) cm^{-1}.

EI-MS *m/z* (%)**:** 214 (10, $[C_{12}H_{24}NO_2]^+$), 172 (20, $[C_7H_8O_3S]^+$), 60 (100, $[C_2H_6NO]^+$).

EI-HRMS (fragment ion $C_{13}H_{28}NO_3$)**:** calculated: 246.20637
measured: 246.20666

ORD (c = 1.04, $CHCl_3$)**:** $[\alpha]_{589}^{20}$ = -7.86; $[\alpha]_{579}^{20}$ = -8.05; $[\alpha]_{546}^{20}$ = -7.91
$[\alpha]_{436}^{20}$ = -14.70; $[\alpha]_{405}^{20}$ = -15.62; $[\alpha]_{365}^{20}$ = -17.60

III.2.2 4-Bromobenzoic acid methyl ester (10)

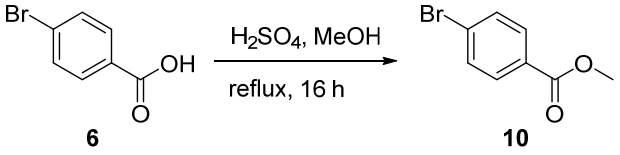

6 **10**

4-Bromobenzoic acid (80.0 g, 0.40 mol, 1.00 eq.) and concentrated sulfuric acid (10.0 mL, 18.4 g, 0.18 mol, 0.45 eq.) were dissolved in methanol (800.0 mL, 632.0 g, 19.73 mol, 49.30 eq.) and refluxed for 16 h. The product mixture was cooled to -20°C and the precipitated solid was separated by filtration. The mother liquor was concentrated *in vacuo* to one third of its volume and again cooled to -20°C. The new precipitated solid was filtrated, combined with the first portion and recrystallized from methanol to give 78.21 g (0.36 mol) of the methyl ester **10** as colourless crystals. Yield 91 %.

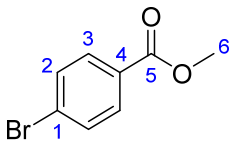

10

^{1}H-NMR ($CDCl_3$, 300 MHz, 300 K): δ = 7.90 (d, 2H, ^3J = 8.0 Hz, 3-H), 7.58 (d, 2H, ^3J = 8.0 Hz, 2-H), 3.91 (s, 3H, 6-H) ppm.

III.2.3 4-Ethynylbenzoic acid (11)

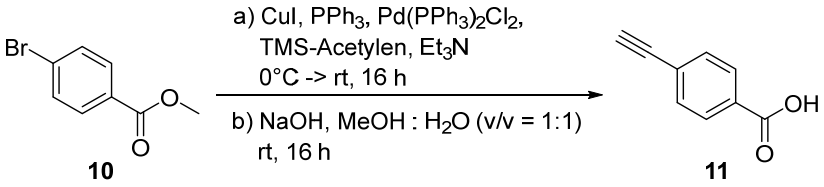

4-Ethynylbenzoic acid **11** was prepared similar to the experimental procedure of Yashima *et* al. [**15**] 4-Bromobenzoic acid methyl ester **10** (36.280 g, 168.7 mmol, 1.00 eq.) was dissolved in 700 mL of a 1:1-mixture (*v/v*) of dry THF and triethylamine. To degas the solution argon was bubbled through it under vigorous stirring over a period of 15 min using a syringe. Then bis(triphenylphosphine)palladium dichloride (1.184 g, 1.7 mmol, 0.01 eq.), triphenylphosphine (0.885 g, 3.4 mmol, 0.02 eq.) and copper(I) iodide (0.643 g, 3.4 mmol, 0.02 eq.) were added and the resulting suspension was cooled to 0°C. After the addition of (trimethylsilyl)acetylene (36.0 mL, 24.9 g, 253.1 mmol, 1.50 eq.) the reaction mixture was slowly warmed to room temperature and stirred for 16 h.

The suspension was filtered over a silica plug and the filtrate concentrated under reduced pressure. 800 mL of a 1:1-mixture (*v/v*) of methanol and 1 N aqueous NaOH were added to the residual methyl-[4-(trimethylsilyl)ethynyl]benzoate and stirred overnight at ambient temperature. After filtration methanol was removed by rotary evaporation and the aqueous solution washed with three portions of methylene chloride and two portions of ether. The aqueous layer was then acidified with 1 N aqueous HCl to pH = 1 and the precipitated solid was separated by filtration. After washing the filter cake with a small amount of water it was dissolved in ethyl acetate. The organic phase was washed with brine, dried over $MgSO_4$ and the solvent was removed *in vacuo* to give 23.238 g (159.0 mmol) of 4-Ethinylbenzoic acid **11** as a bronze coloured solid. Yield 94 % over two steps.

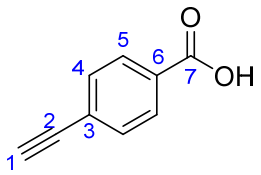

11

^{1}H-NMR: (DMSO-d$_6$, 300 MHz, 300 K): δ = 13.14 (bs, 1H, COOH), 7.93 (d, 2H, ^3J = 8.2 Hz, 5-H), 7.59 (d, 2H, ^3J = 8.2 Hz, 4-H) 4.43 (s, 1H, 1-H) ppm.

III.2.4 *N*-Hydroxysuccinimidyl-4-ethynylbenzoate (12)

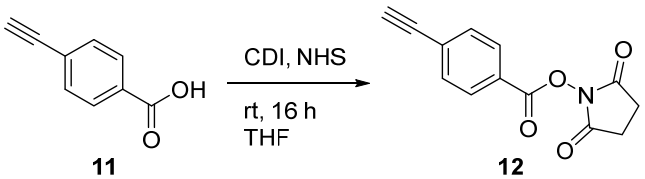

11 **12**

4-Ethynylbenzoic acid **11** (20.00 g, 136.9 mmol, 1.0 eq.) and *N*-Hydroxysuccinimide (17.33 g, 150.5 mmol, 1.1 eq.) were dissolved in 500 mL THF. Afterwards 1,1'-Carbonyldiimidazole (28.85 g, 177.9 mmol, 1.3 eq.) was added portionwise under gas evolution. The reaction mixture was stirred for 16 h at ambient temperature. The solvent was removed by rotary evaporation and the solid residue suspended in water with the help of sonification. The solid was separated by filtration, washed with water and dried *in vacuo* to give 30.010 g (123.4 mmol) of the active ester **12** as a light yellow powder. Yield 90 %.

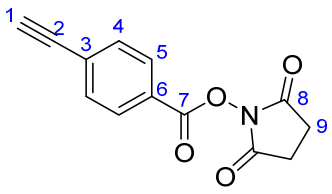

12

^{1}H-NMR: (DMSO-d$_6$, 300 MHz, 300 K): δ = 8.08 (d, 2H, ^3J = 8.6 Hz, 5-H), 7.73 (d, 2H, ^3J = 8.6 Hz, 4-H), 4.62 (s, 1H, 1-H), 2.9 (s, 4H, 9-H) ppm.

III.2.5 *N*-(4-Ethynyl)benzoyl-L-serine decyl ester (13)

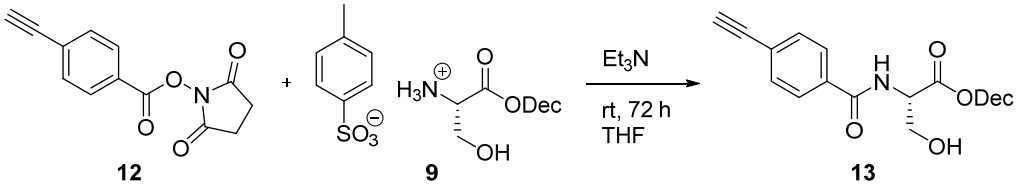

To *N*-Hydroxysuccinimidyl-4-ethynylbenzoate **12** (9.708 g, 39.9 mmol, 1.0 eq.) and *L*-Serine decyl ester hydrotosylate **9** in 300 mL THF was added triethylamine (7.2 mL, 5.3 g, 51.9 mmol, 1.3 eq.). After stirring the resulting solution for 72 h at ambient temperature the solvent was removed by rotary evaporation and the residue taken up in 100 mL methylene chloride. The organic phase was washed with 50 mL of 1 N aqueous HCl, dried over $MgSO_4$ and evaporated to dryness. The crude product was purified by flash column chromatography (elution with mixtures of petroleum ether: ethyl acetate = 3:1, 1:1, 1:2 (*v/v*)) to afford the amide **13** (11.918 g, 31.91 mmol) as a colourless solid. Yield 80 %.

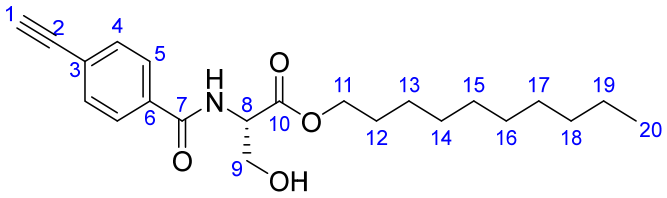

13

T_m = 98°C.

^{1}H-NMR: ($CDCl_3$, 300 MHz, 300 K): δ = 7.78 (d, 2H, ^3J = 8.5 Hz, 5-H), 7.55 (d, 2H, ^3J = 8.5 Hz, 4-H), 7.13 (d, 1H, ^3J = 7.1 Hz, NH), 4.83 (dt, 1H, ^3J = 7.1 Hz, ^3J = 3.6 Hz, 8-H), 4.20 (t, 2H, ^3J = 6.7 Hz, 11-H), 4.05 (d, 2H, ^3J = 3.6 Hz, 9-H), 3.21 (s, 1H, 1-H), 2.41 (bs, 1H, OH), 1.67 ("quint", 2H, 12-H), 1.17 – 1.42 (m, 14H, 13,14,15,16,17,18,19-H), 0.88 (t, 3H, ^3J = 6.7 Hz, 20-H) ppm.

^{13}C-NMR: ($CDCl_3$, 125 MHz, 300 K): δ = 170.7 (10-C), 167.0 (7-C), 133.6 (6-C), 132.4 (4-C), 127.3 (5-C), 126.0 (3-C), 82.8 (2-C), 79.9 (1-C), 66.4 (11-C), 63.5 (9-C), 55.5 (8-C), 32.0 (18-C), 29.6 + 29.6 + 29.4 (15,16,17-C), 29.3 (14-C), 28.6 (12-C), 25.9 (13-C), 22.8 (19-C), 14.2 (20-C) ppm.

IR (KBr)**:** $\tilde{\nu}$ = 3346 (-CONH), 2919 (-CH_2), 2853 (-CH_2), 1746 (-COOR), 1623 (-CONH) cm^{-1}.

EI-MS *m/z* (%)**:** 356 (4, $[C_{22}H_{30}NO_3]^+$), 170 (21, $[C_{11}H_8NO]^+$), 129 (100, $[C_9H_5O]^+$).

ESI-HRMS ($C_{22}H_{31}NO_4$)**:** calculated: m/z = 396.21453 $[M+Na]^+$
measured: m/z = 396.21494 $[M+Na]^+$

EA ($C_{22}H_{31}NO_4$)**:** calculated: C 70.75 H 8.37 N 3.75
measured: C 70.64 H 8.37 N 3.74

ORD (c = 1.04, $CHCl_3$)**:** $[\alpha]_{589}^{20}$ = 43.37; $[\alpha]_{579}^{20}$ = 45.64; $[\alpha]_{546}^{20}$ = 53.37
$[\alpha]_{436}^{20}$ = 93.16; $[\alpha]_{405}^{20}$ = 116.59; $[\alpha]_{365}^{20}$ = 162.18

III.2.6 *N*-(4-Ethynyl)benzoyl-*O*-anisoyl-L-serine decyl ester (2)

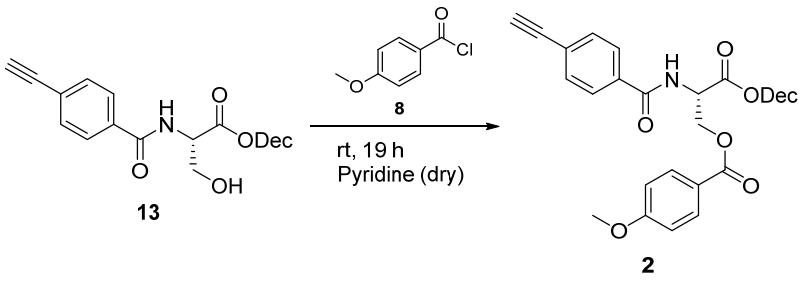

Inspired by the literature **[16]**, *N*-(4-Ethynyl)benzoyl-L-serine decyl ester **13** (1.00 g, 2.7 mmol, 1.0 eq.) was dissolved in dry pyridine (11.0 mL, 10.8 g, 136.3 mmol, 50.5 eq.) and cooled to 0°C. After the addition of *p*-anisoyl chloride **8** (0.50 g, 3.0 mmol, 1.1 eq.) the reaction mixture was warmed to room temperature and stirred for 19 h. After ensuring the complete conversion of **13** by TLC control, the solvent was removed by rotary evaporation and the residue taken up in 25 mL ethyl acetate. The organic phase was washed with 25 mL of saturated aqueous $NaHCO_3$, 1 N aqueous HCl and brine respectively, dried over $MgSO_4$ and evaporated to dryness. After recrystallization of the crude product (1.435 g) from *n*-hexane / ethyl acetate the monomer **2** (1.285 g, 2.53 mmol) was obtained as a colourless, crystalline solid. Yield 95 %.

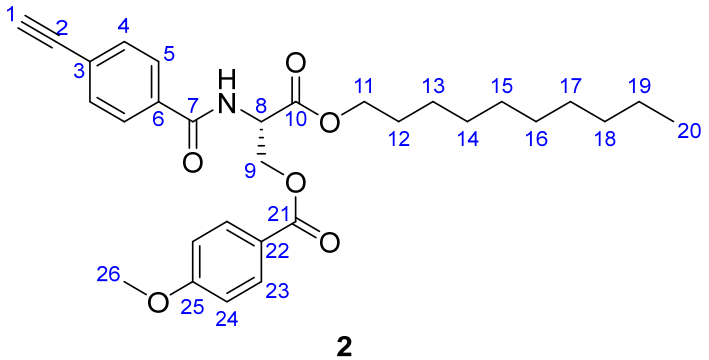

2

T_m = 88°C

^{1}H-NMR: ($CDCl_3$, 500 MHz, 300 K): δ = 7.94 (d, 2H, ^3J = 8.9 Hz, 23-H), 7.77 (d, 2H, ^3J = 8.2 Hz, 5-H), 7.54 (d, 2H, ^3J = 8.2 Hz, 4-H), 7.14 (d, 1H, ^3J = 7.4 Hz, NH), 6.90 (d, 2H, ^3J = 8.9 Hz, 24-H), 5.11 (dt, 1H, ^3J = 7.4 Hz, ^3J = 3.7 Hz, 8-H), 4.73 (d, 2H, ^3J = 3.7 Hz, 9-H), 4.24 (dt, 1H, ^3J = 10.7 Hz, ^3J = 6.7 Hz, 11b-H), 4.17 (dt, 1H, ^3J = 10.7 Hz, ^3J = 6.7 Hz, 11a-H), 3.84 (s, 3H, 26-H), 3.20 (s, 1H, 1-H), 1.62 („quint“, 2H, 12-H), 1.15 – 1.35 (m, 14H, 13,14,15,16,17,18,19-H), 0.87 (t, 3H, ^3J = 7.1 Hz, 20-H) ppm.

^{13}C-NMR: ($CDCl_3$, 125 MHz, 300 K): δ = 169.77 (10-C), 166.41 (7-C), 166.14 (21-C), 163.90 (25-C), 133.73 (6-C), 132.43 (4-C), 131.92 (23-C), 127.26 (5-C), 125.91 (3-C), 121.77 (22-C), 113.90 (24-C), 82.83 (2-C), 79.79 (1-C), 66.48 (11-C), 64.43 (9-C), 55.55 (26-C), 52.94 (8-C), 31.97 (18-C), 29.62 + 29.55 + 29.38 (15,16,17-C), 29.28 (14-C), 28.64 (12-C), 25.90 (13-C), 22.77 (19-C), 14.20 (20-C) ppm.

IR (KBr)**:** $\tilde{\nu}$ = 3279.2 (-CONH) 3067.8 (=C-H), 2924.9 (-CH_2), 2853.5 (-CH_2), 1731.1 (-COOR), 1631.6 (-CONH), 1608.2 (aromatic ring vibration) cm^{-1}.

EI-MS *m/z* (%)**:** 507 (2, $[M]^+$), 372 (7, $[C_{22}H_{30}NO_4]^+$), 355 (22, $[C_{22}H_{29}NO_3]^+$), 170 (39, $[C_{11}H_8NO]^+$), 135 (100, $[C_8H_7O_2]^+$), 129 (85, $[C_9H_5O]^+$), 101 (13, $[C_8H_5]^+$).

EI-HRMS (fragment ion $C_{30}H_{37}NO_6$)**:** calculated: m/z = 507.2615 $[M]^+$

measured: m/z = 507.2597 $[M]^+$

EA ($C_{30}H_{37}NO_6$)**:**	calculated:	C 70.98	H 7.35	N 2.76
	measured:	C 70.92	H 7.28	N 2.83

ORD (c = 1.05, $CHCl_3$)**:** $[\alpha]_{589}^{20}$ = 75.36; $[\alpha]_{579}^{20}$ = 79.23; $[\alpha]_{546}^{20}$ = 93.39

$[\alpha]_{436}^{20}$ = 188.60; $[\alpha]_{405}^{20}$ = 246.64; $[\alpha]_{365}^{20}$ = 387.01

III.3 Polymerization

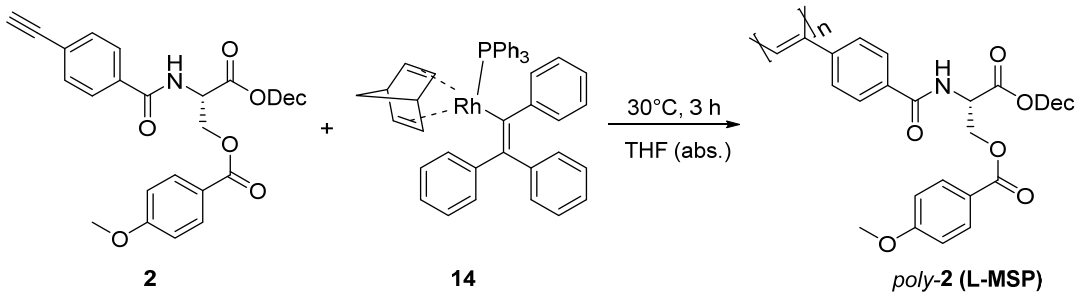

2 **14** *poly*-**2 (L-MSP)**

The vinyl rhodium complex **14**, originally introduced by MISUMI and MASUDA, was adapted for the polymerization of monomer **2** [**17**]. The synthesis of the catalyst **14** was achieved in two steps starting from triphenylvinyl bromide and lithium as already shown in a former publication [**1**].

A flame-dried flask was charged with 9 g (17.73 mmol) of the monomer **2** and dissolved in 88.7 mL of absolute THF to yield a monomer concentration of 0.2 mol/L. The solution was heated to 30°C and 2.36 mL (23.6 µmol) of a 0.01 M catalyst solution in THF/diethylether was added rapidly via syringe under vigorous

stirring. The reaction mixture with a monomer to initiator ratio of 750:1 was stirred rapidly over the course of 3 h at 30°C. Afterwards the living chain ends were terminated by the addition of 1.0 mL of acetic acid. Stirring was continued for additional 20 min.

The resulting yellow, viscous solution was transferred dropwise into 1.7 L of methanol under constant shaking whereupon precipitation of the polymer occurred. After separation by centrifugation the obtained yellow solid was dissolved again in about 100 mL of THF and then again precipitated in 1.7 L of methanol. The polymer was centrifuged, dried *in vacuo*, taken up in 125 mL of benzene and lyophilized to yield 8.719 g of a yellow solid of spongy consistency. Yield 97 %.

III.4 Analytical data of *poly*-2 (*L*-MSP)

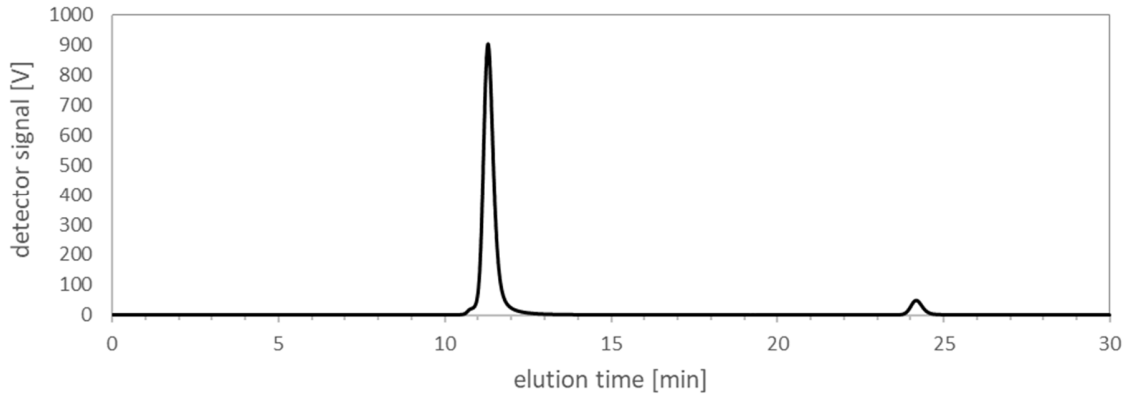

Figure SI-5. SEC of poly-**2**. THF containing 0.1 wt-% of tetrabutylammonium bromide (TBAB) was used as mobile phase. The peak at about 24 min is caused by toluene which served as a reference.

Table SI-1. **Optical rotatory dispersion (**ORD) measurements of *poly*-9 (*L*-MSP)

Polymer	$[\alpha]_{589}^{20}$ a)	$[\alpha]_{578}^{20}$ a)	$[\alpha]_{546}^{20}$ a)	c b) [mg/cL]
p#9	-526.2	-576.2	-700.0	0.10

a) Optical rotatory dispersion at T=20°C and wavelength λ; b) Concentration of ORD samples in $CHCl_3$.

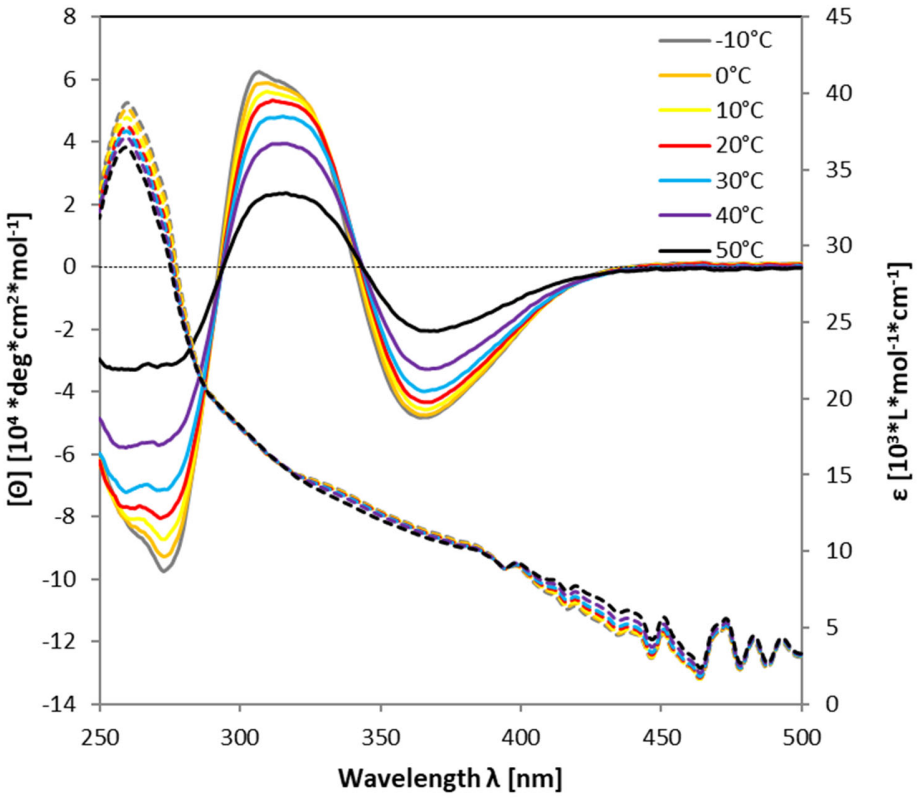

Figure SI-6. Temperature dependent UV (dashed lines) and CD spectra (solid lines) of *poly*-**2** dissolved in $CHCl_3$ (3.95 mg / 250 mL).

IV. Oriented sample preparation

The chiral LLC's investigated in this work were prepared using helical polymers of PBLG, PCBLL, PDA and L-MSP (see Introduction) and $CHCl_3$ or DMF (see below) as a weakly-polar organic co-solvent. Each of them forms homogeneous and uniform chiral anisotropic media of nematic type in a sufficiently intense magnetic field.

All oriented samples were prepared according to the same (optimized) protocol. The *D*- and *L*-camphor and then the polymer are weighed directly into the 5 mm NMR tube. Finally, the co-solvent is added and the tube is then sealed to avoid evaporation of the solvent over time. The tube is then stirred upside down several times, in order to obtain a homogeneous phase without material concentration gradient. The sample (PCBLL) can be slightly heated to facilitate the dissolution of the polymer (solid) and the homogenization of the mixture.

In **Table SI-2** is listed the exact sample composition of oriented samples of **5** dissolved in LLCs made of PDA (**1**), L-MSP (**2**), PBLG (**3**) and PCBLL (**4**), with the condition m_{poly}/m_{Tot} = 19% for all of them. For the sample with the PCBLL, chloroform was replaced by a more polar co-solvent (DMF) because the use

of chlorinated co-solvents, either $CHCl_3$ or CH_2Cl_2, (with the chosen polymer ratio) leads to a gel phase inducing broad line-shapes with a significant reduction of S/N ratio.

Table SI-2. Exact composition of four oriented samples studied

Sample	Polymer	DP [a]	$m_{poly.}$ (mg)	m_{CHCl3} (mg)	m_{DMF} (mg)	$m_{anal.}$ (*D*) (mg)	$m_{anal.}$ (*L*) (mg)	$m^{Tot}_{anal.}$ (mg)	$m_{poly.}/m_T$ (%)	*ee(D)*[b] (%)
1	**PDA**	750	149.9	590.1	-	26.3	14.0	40.3	19.1	30.5
2	**L-MSP**	750	149.4	591.0	-	26.3	14.2	40.5	19.3	29.9
3	**PBLG**	768	151.3	589.3	-	26.6	14.2	40.8	19.4	30.4
4	**PCBLL** [c]	778	94.9	-	363.3	26.1	15.1	41.2	19.0	26.7

[a] Degree of polymerization (DP) of polymer. [b] The major enantiomer is the (*D*)-(1*R*,4*R*)-(+)-camphor (**5**). [c] To keep similar the length of this oriented sample compared to other ones (and the spin density detected by the coil), the mass of polymer and co-solvent have been reduced, but keeping the $m_{poly.}/m_T$ ratio constant and equal to 19%.

In **Table SI-3** is listed the various physical parameters of *L*- and *D*-enantiomers of **5** in the PDA (**1**), L-MSP (**2**), PBLG (**3**) and PCBLL (**4**), mesophases studied and compared.

Table SI-3. Physical parameters of four oriented samples studied

Sample	Poly. [a]	$MW_{unitpoly}$ [b] ($g.mol^{-1}$)	MW_{poly} [c] ($kg.mol^{-1}$)	n^D [d] ($\times10^{-5}$ mol)	n^L [d] ($\times10^{-5}$ mol)	$[^2H]_i^D$ [e] ($\times10^{-5}$ mol/l)	$[^2H]_i^D$ [e] ($\times10^{-5}$ mol/l)	$X^D_{sol/unitpol}$ [f] (no unit)	$X^L_{sol/unitpoly}$ [f] (no unit)
1	**PDA** (~750)	385 ($C_{24}H_{35}NO_3$)	289	17.3	9.20	~ 6.7	~ 3.6	0.43	0.23
2	**L-MSP** (~750)	507 ($C_{30}H_{37}NO_6$)	380	17.3	9.33	~ 6.7	~3.6	0.56	0.30
3	**PBLG** (~768)	219 ($C_{12}H_{13}NO_3$)	~168	17.5	9.33	~ 6.8	~ 3.6	0.25	0.14
4	**PCBLL** (~778)	262 ($C_{14}H_{18}N_2O_3$)	~204	17.1	9.92	~6.9	~ 4.0	0.47	0.27

[a] Chiral polymer used. In parenthesis are given the DPs of polymer provided by the supplier (determination by viscosity). [b] Molar weight for the polymeric unit. [c] Molar weight of polymer (in $kg.mol^{-1}$). The values for **3** and **4** are provided by the supplier (determination by viscosity and LALLS, respectively). [d] Molar amount of (*D*/*L*)-analytes (MW = 152.2 $g.mol^{-1}$). [e] Molar concentration in analyte monodeuterated isotopomers. Values must be tripled for methyle sites *i* consisting of homotopic (equivalent) deuterons (sites 8, 9 and 10). [f] Ratio between the number of analytes monodeuterated isotopomers and the number of monomer units of the polymer. Values must be tripled for sites *i* consisting of homotopic (equivalent) deuterons (sites 8, 9 and 10).

V. The ^2H-{^1H} *Q*-resolved Fz 2D experiments

The ANAD 2D-NMR spectra of **5** dissolved in the four chiral LLCs were recorded with the 2D *Q*-resolved Fz pulse sequence (**Figure SI-7**). This QUOSY-type 2D sequence allows the refocusing of ^2H chemical shifts during t_1. After a double FT, only the ^2H-QDs are observed in the dimension F_1. Due to the z-filter (α_n-G_z- α_n) incorportated after the t_1 evolution period, the *Q*-resolved Fz 2D spectra can be phased in pure absorption mode. 2D maps can be tilted and then symmetrized. After the tilting process, the ^2H-QDs are formally eliminated ("decoupled") in spectral dimension F_2, leading to a pure-shift spectral dimension.

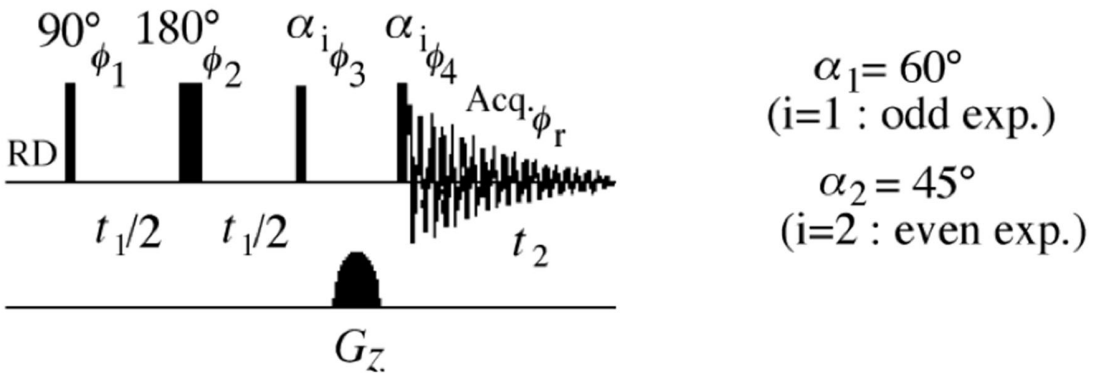

Figure SI-7. Pulse diagram of the 2D *Q*-resolved Fz sequence. The phase cycling is ϕ_1 = 4(x); ϕ_2 = x, y, -x, -y; ϕ_3 = ϕ4 = 4(x); ϕ_r =2(x, -x). The CPD-type proton decoupling (not shown) is applied during all the sequence.

VI. The $^1T_{CH}$-resolved 2D experiments

Figure SI-8 shows the 2D heteronuclear ($^1T_{CH}/2$)-resolved and phased ($^1T_{CH}/4$)-resolved sequences that can be used to analyze the CH_2 groups and extract the total coupling constants, ($^1T_{CH}/2$) and $^1T_{CH}/4$, respectively [**1**]. Interestingly, this experiment allows to simply correlate the $^1T_{CH}$ information to each ^{13}C peak for the *L*- and *D* enantiomers of camphor.

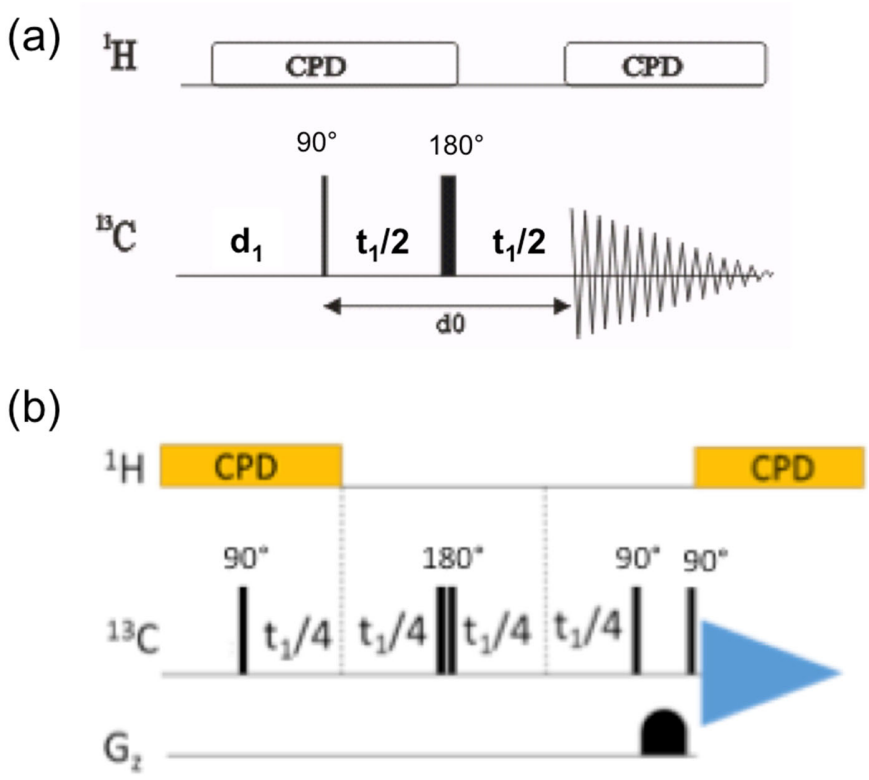

Figure SI-8. (a) Pulse diagram of two *T*- or *J*-resolved-type heteronuclear 2D sequences: (a) the classical ($^1T_{CH}/2$-resolved sequence ("magnitude mode" 2D map); (b) the ($^1T_{CH}/4$)-resolved sequence ("phased" 2D map) [**2**].

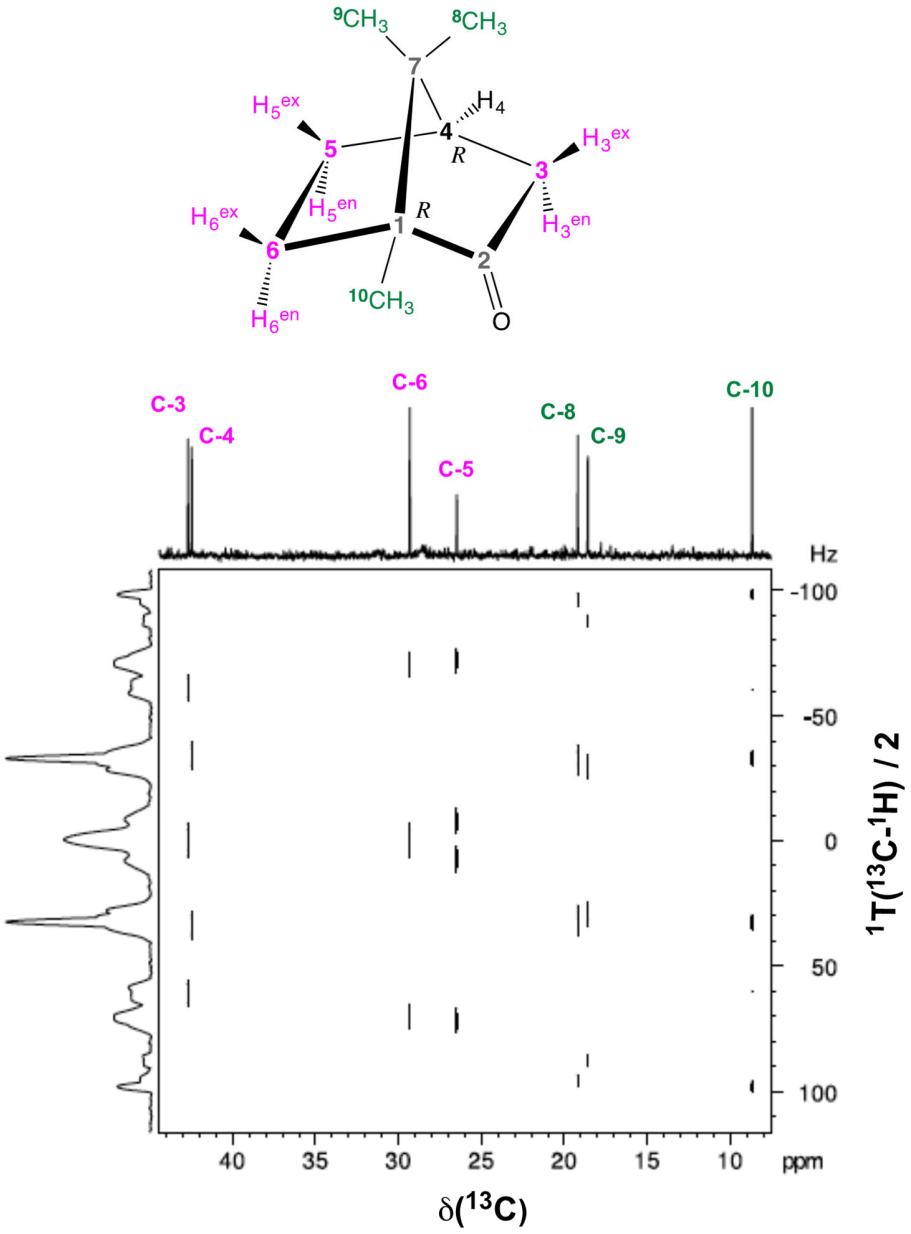

Figure SI-9. One example of experimental ($^1T_{CH}/2$)-resolved 2D spectrum with associated F_1/F_2 projections of **5** dissolved in *L*-MSP mesophase recorded with the pulse-sequence of **Figure SI-8a**.

VII. DFT-based structure of camphor

All back-calculated ^{2}H-RQC data for *R* and *S* enantiomers of camphor presented in this work have been obtained from fitting the ^{2}H-RQC data against the structure of (-)-*L*-(*S*,*S*)-camphor. The atomic coordinates for (-)-*L*-(*S*,*S*)-camphor have been computed based on DFT optimizations at the B3LYP/6-311+G(d,p) level of theory. They are listed in **Table SI-4**.

This protocol is valid because all anisotropic NMR properties are inversion invariant. This means that we obtain the same numbers for all quantities calculated with the input geometry of (+)-*D*-(*R*,*R*)-

Table SI-4. Computed atomic coordinates of the (*L*)-(*S*,*S*)-camphor [a]

Atom	x	y	z
C_1	-0.294679	-0.506866	-0.548868
C_2	-1.443429	+0.058897	+0.287158
C_3	-0.875475	+1.244584	+1.072207
C_4	+0.591968	+1.268630	+0.598365
C_5	+0.575365	+1.786937	-0.858299
C_6	-0.077093	+0.604328	-1.635071
C_7	+0.918356	-0.251634	+0.421787
C_8	+0.841612	-1.068243	+1.724740
C_9	+2.293974	-0.518676	-0.207343
C_{10}	-0.528659	-1.900733	-1.099439
H_3^{en}	-1.431455	+2.158220	+0.845988
H_3^{ex}	-0.985699	+1.057640	+2.143251
H_4	+1.267175	+1.809638	+1.263618
H_5^{en}	+0.000233	+2.711372	-0.946860
H_5^{ex}	+1.581738	+1.998892	-1.222836
H_6^{en}	-1.017687	+0.879192	-2.118292
H_6^{ex}	+0.578618	+0.215775	-2.417021
H_{8a}	+1.033018	-2.125669	+1.521965
H_{8b}	-0.124057	-1.007323	+2.230208
H_{8c}	+1.606277	-0.727413	+2.429510
H_{9a}	+2.443412	-1.590770	-0.363504
H_{9b}	+2.443720	-0.022093	-1.166095
H_{9c}	+0.082760	-0.174898	0.469429
H_{10a}	-0.679097	-2.629244	-0.298503
H_{10b}	+0.320240	-2.227742	-1.705815
H_{10c}	-1.420935	-1.920213	-1.730634
O	-2.588738	-0.338588	+0.316771

[a] Atomic coordinates are given in Angström unit.

camphor (inversion of coordinates of (-)-*L*-(*S*,*S*)-camphor (x,y,z -> -x,-y,-z)). Note however that switching between *D*- and *L*-camphor geometries by mirroring only affects the calculation of the GCB inter-tensor angles. In order to avoid any dependencies of the GCB values on the orientation of the analyte structure, it is preferable to use a single enantiomer for a specific chiral analyte structure.

VIII. Isotropic ^{13}C and ^{13}C-{^{1}H} and ^{2}H-{^{1}H} 1D-NMR spectra of camphor (5)

Figures SI-10a, b reports the isotropic ^{13}C proton-decoupled (^{13}C-{^{1}H}) and the ^{13}C proton-coupled (^{13}C) 1D spectra of **5** were recorded at 100.4 MHz in $CHCl_3$ (δ = 77.0 ppm). From the ^{13}C proton-coupled NMR spectrum are extracted the $^{1}J_{CH}$ scalar coupling constants where signs are assumed to be always positive. These scalar constants will then be used to determine the sign of the dipolar coupling constants, $^{1}D_{CH}$, from the total C-H couplings, $^{1}T_{CH}$, measured on the anisotropic ^{13}C 1D or 2D spectrum (in the four phases). Finally, **Figure SI-11** shows the isotropic ^{2}H proton-decoupled (^{2}H-{^{1}H}) 1D spectrum of **5** recorded at 92.1 MHz.

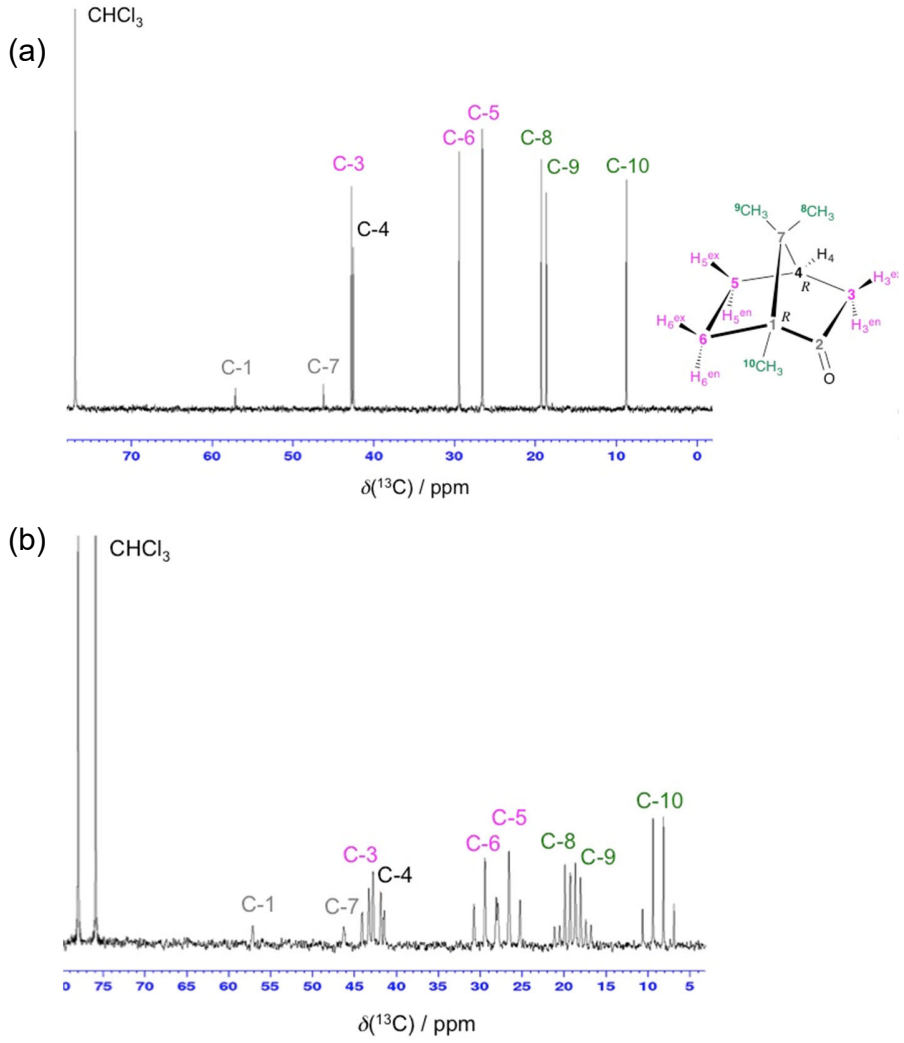

Figure SI-10. (a) 100.3 MHz ^{13}C-{^{1}H} 1D-NMR spectrum and (b) ^{13}C spectrum of **5** in an isotropic solution of chloroform (at 300 K). 256 and 600 scans were added, respectively.

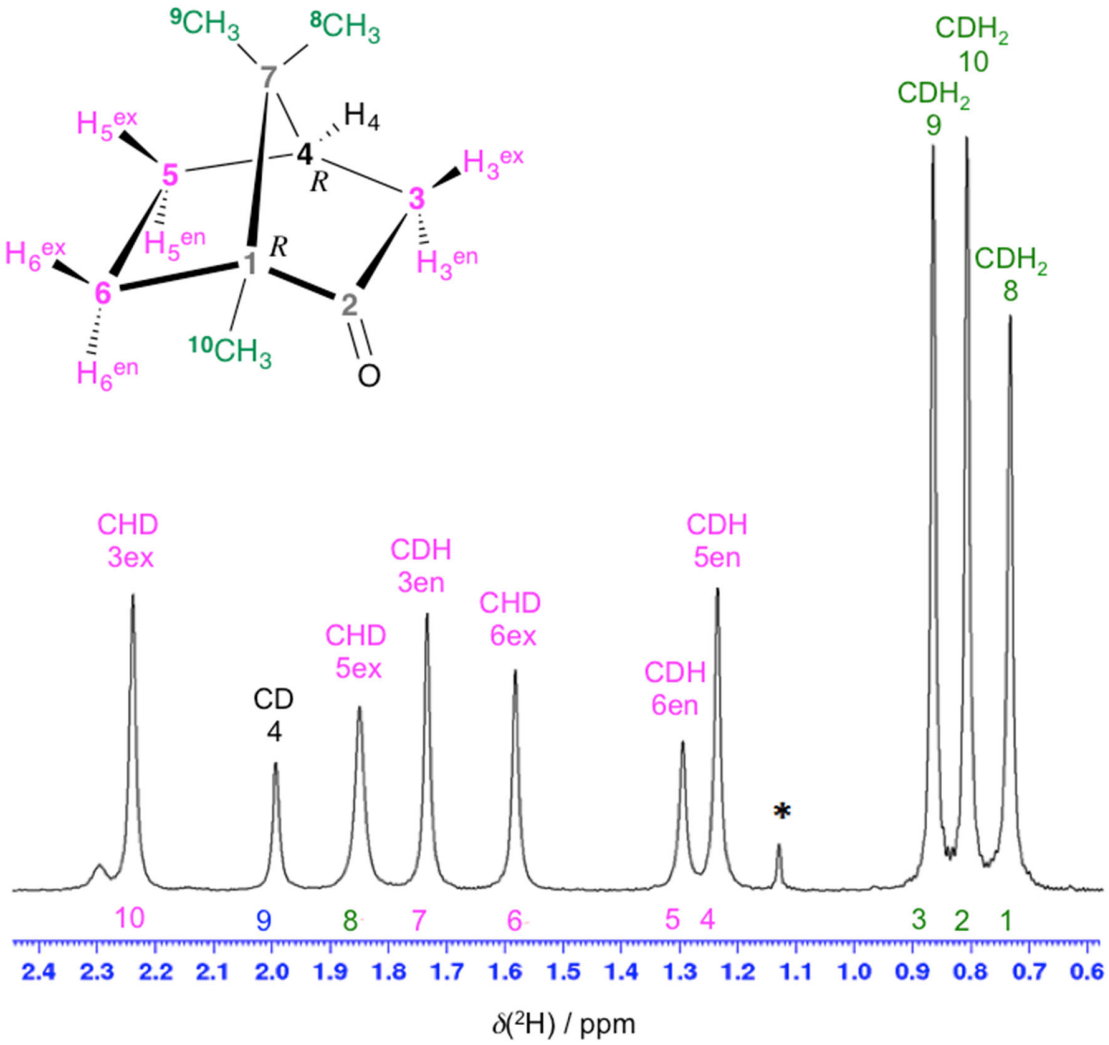

Figure SI-11. 92.1 MHz ^{2}H-{^{1}H} 1D-NMR spectrum of **5** in an isotropic solution of protonated chloroform (at 300 K). 3000 scans were added. Exponential filtering (LB = 2 Hz) was applied. The asterisked peak corresponds to the NAD signal of methyl group of ethanol used as a stabilizer of chloroform. Note that in DMF, ^{2}H peaks located between 1.2 and 1.3 ppm (CHD(6_{en}) and CHD(5_{en}) are inverted.

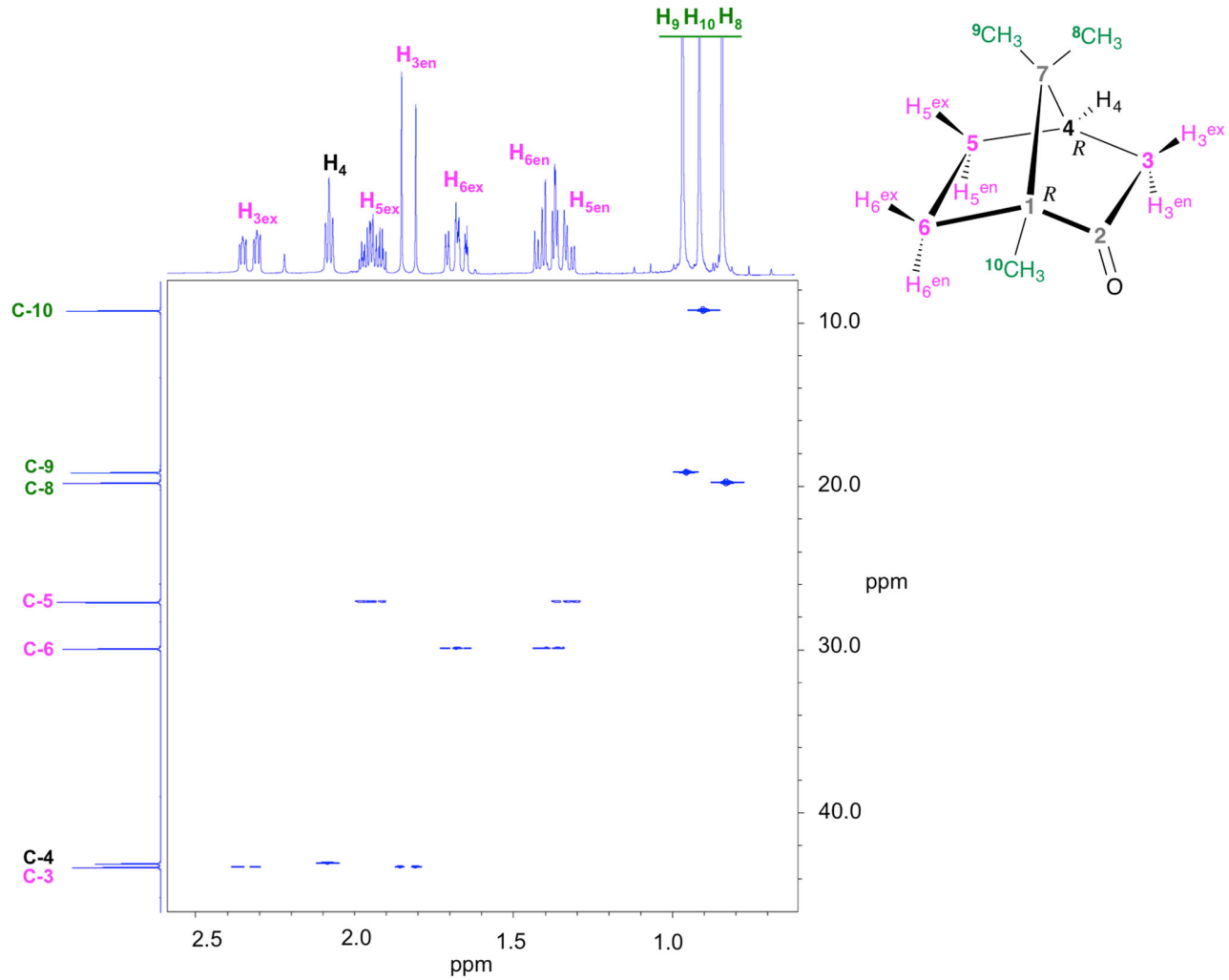

Figure SI-12. Isotropic 100.3 MHz ^{1}H-^{13}C HSQC 2D spectrum of **5** recorded in $CDCl_3$ at 300 K. The 2D map was acquired with 2048 (t_2) × 512 (t_1) data points and zero-filled to 4k(t_2) × 4k (t_1) data points with 128 scans per t_1 increment and a recycling delay of 2.3 s. Exponential filtering applied ($LB_{1,2}$ = 2 Hz). The ^{13}C-{^{1}H} and the residual ^{1}H signal chloroform are calibrated at 77.0 and 7.27 ppm, respectively. On the F_2 and F_1 projections are displayed the ^{1}H and ^{13}C-{^{13}H} 1D spectra, respectively.

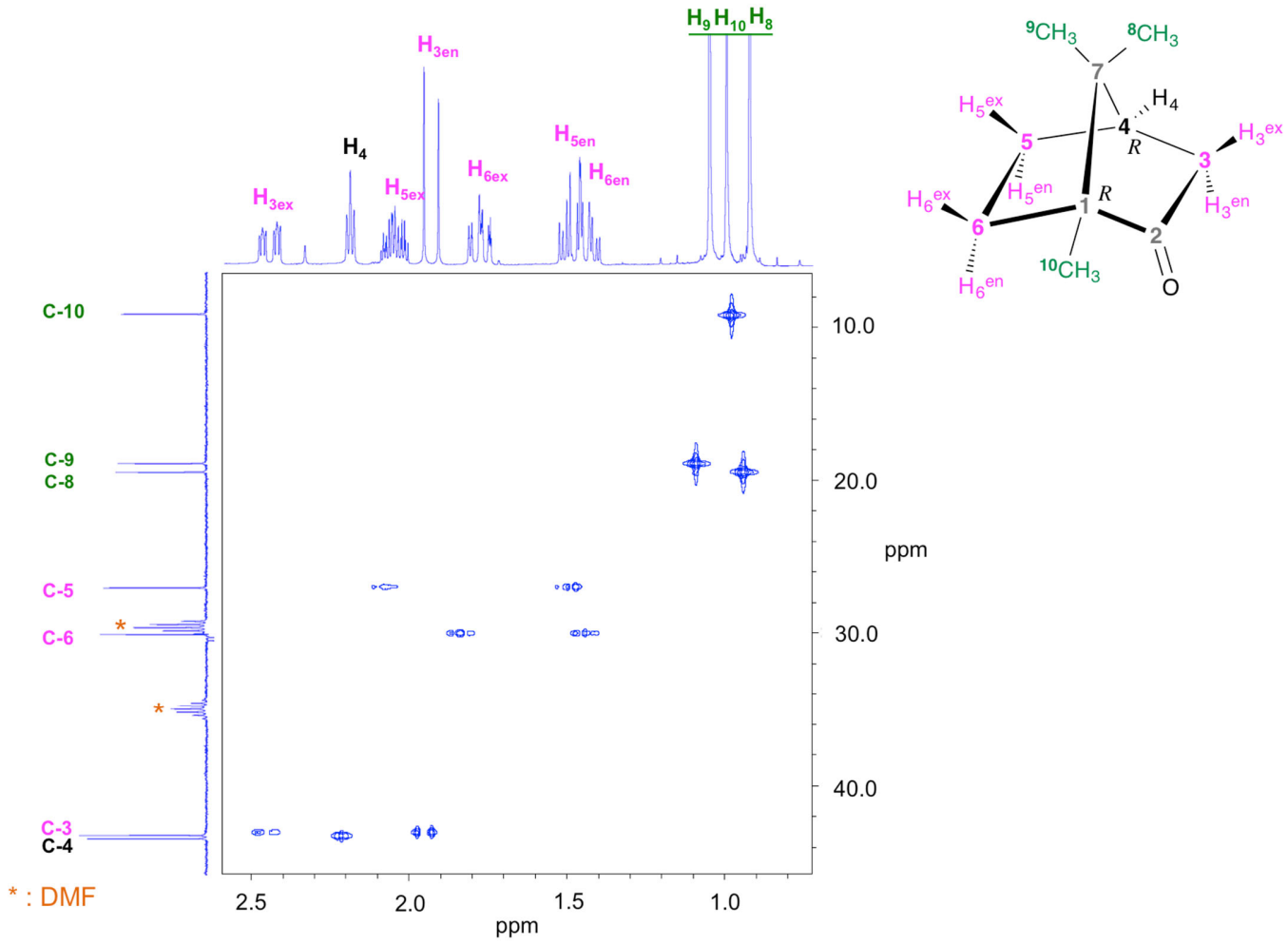

Figure SI-13. Isotropic 100.3 MHz ^{1}H-^{13}C HSQC 2D spectrum of **5** recorded in DMF-d$_7$ at 300 K. Experimental parameters are same as HSQC shown in Figure SI-8. The ^{13}C-{^{1}H} and residual ^{1}H signal of DMF (the most shielded CH$_3$) are calibrated at 29.76 and 2.88 ppm, respectively. On the F_2 and F_1 projections are displayed the ^{1}H and ^{13}C-{^{13}H} 1D spectra, respectively. Note the inversion of H$_{5en}$ and H$_{6en}$ peaks as well as C-3 and C-4 peaks compared to CDCl$_3$ (see **Figure SI-10**).

IX. The NAD *Q*-resolved 2D maps of (*L*)- and (*D*)-camphor (5) in the PBLG and PCBLL mesophases

In this section are given the *Q*-resolved 2D maps of (*L*)- and (*D*)-camphor (**5**) in the PBLG/CHCl$_3$ and PCBLL/DMF mesophases with a zoom of the methyl region (**Figures SI-14** and **SI-15**).

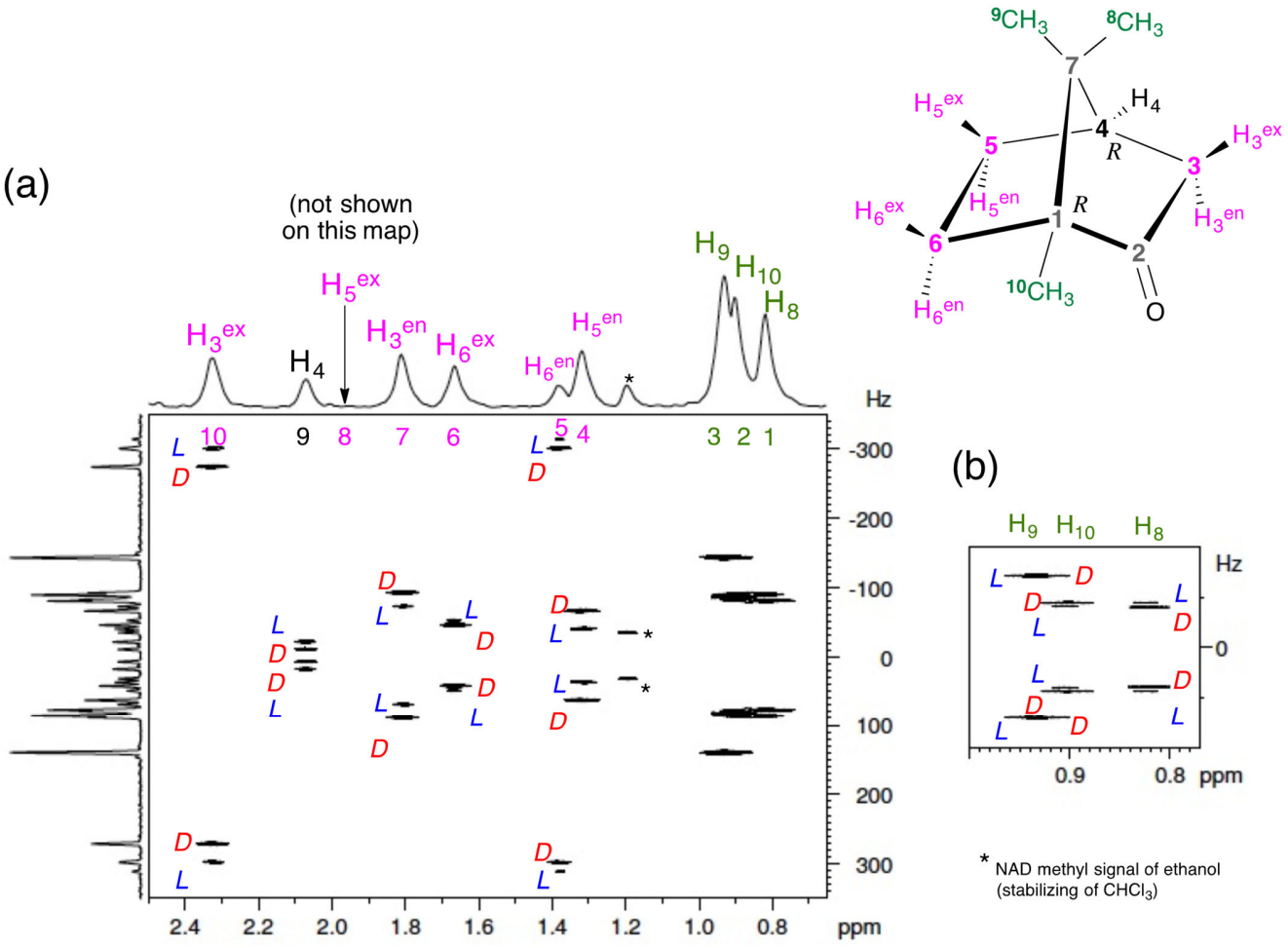

Figure SI-14. (a) 92.1 MHz NAD-{^{1}H} *Q*-resolved Fz 2D spectrum (tilted and then symmetrized) of **5** (ee(*D*) = 30%) in PBLG/$CHCl_3$, showing the assignment of QDs accordingly to atomic numbering of **Figure 1** (see article) as well as the stereodescriptors *L*/*D* for each ^{2}H-QD. (b) Zoom on the methyl region. The ANAD 2D map was acquired with 2200 (t_2) × 400 (t_1) data points (4k × 4k data points as SI), 128 scans per t_1 increment and a recycling delay of 0.7 s. Exponential filtering applied ($LB_{1,2}$ = 1.5 Hz). Due to their magnitude ($\Delta\nu_Q$ > 1 KHz), the NAD (*L*/*D*)-signals at site H_{5ex} is not shown.

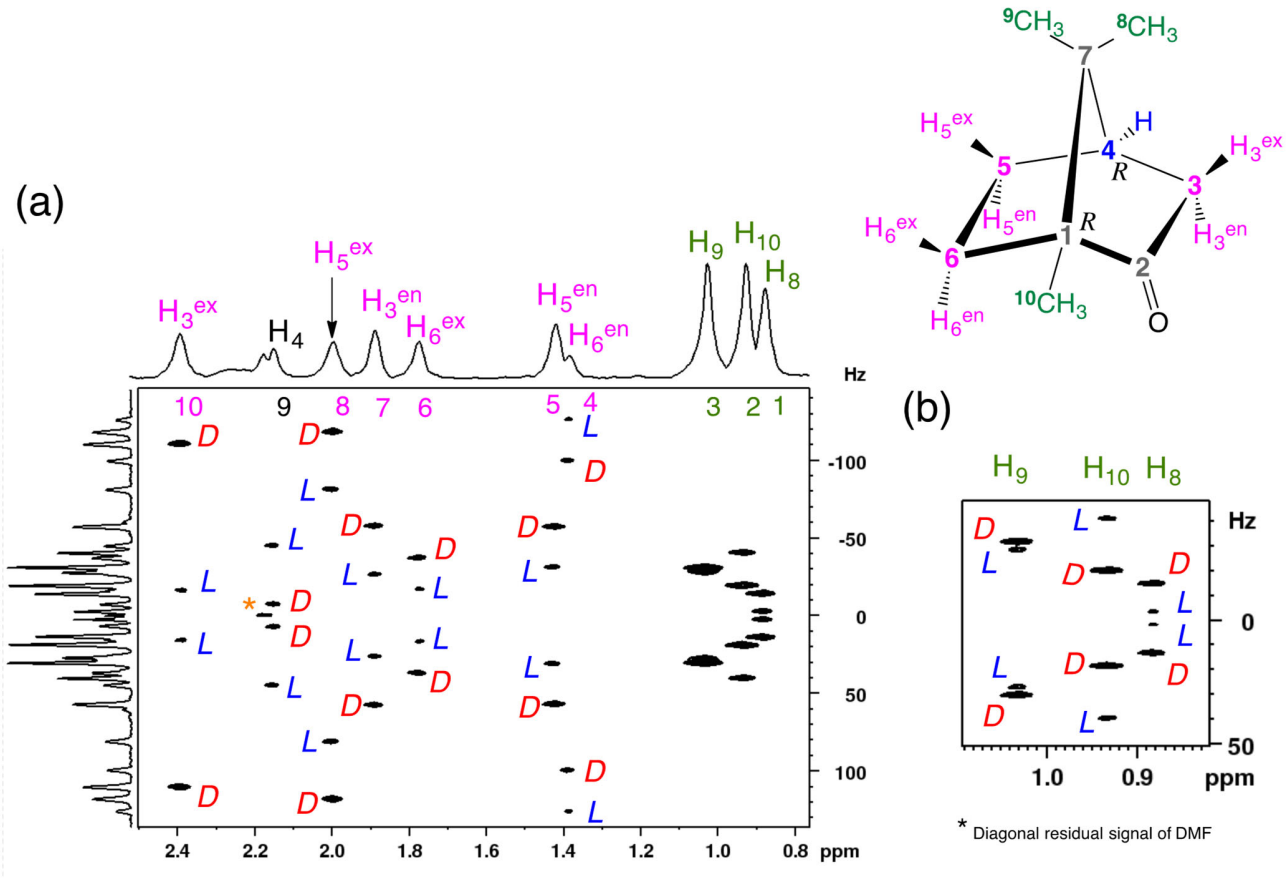

Figure SI-15. (a) 92.1 MHz NAD-{^{1}H} *Q*-resolved Fz 2D spectrum (tilted and then symmetrized) of **5** (ee(*D*) = 30%) in PCBLL/DMF, showing the assignment of QDs accordingly to atomic numbering of **Figure 1** (see article), as well as the stereodescriptors *L*/*D* for each ^{2}H-QD. (b) Zoom on the methyl region. The ANAD 2D map was acquired with 2200 (t_2) × 400(t_1) data points (4k × 4k datapoints as SI), 128 scans per t_1 increment and a recycling delay of 0.7 s. Exponential filtering applied ($LB_{1,2}$ = 1.5 Hz). The NAD signals of the H_5^{en} and H_6^{en} sites are inversed in comparison with the positions observed in the 2D NAD maps recorded in the PDA, *L*-MSP and PBLG mesophases in accordance with the spectral attribution given in the Section IX.

X. Analysis of methylene groups (*D*)- and (*L*)-camphor (5) in the *L*-MSP mesophase

In this Section, we schematically depict the analysis of the methylene groups of **5** (prostereogenic carbons C-3, C-5 and C-6) whose two internuclear directions ^{13}C-^{1}H (^{13}C-^{2}H) are inequivalent (diastereotopic directions). These explicative schemes derived from experimental NMR spectra (not shown).

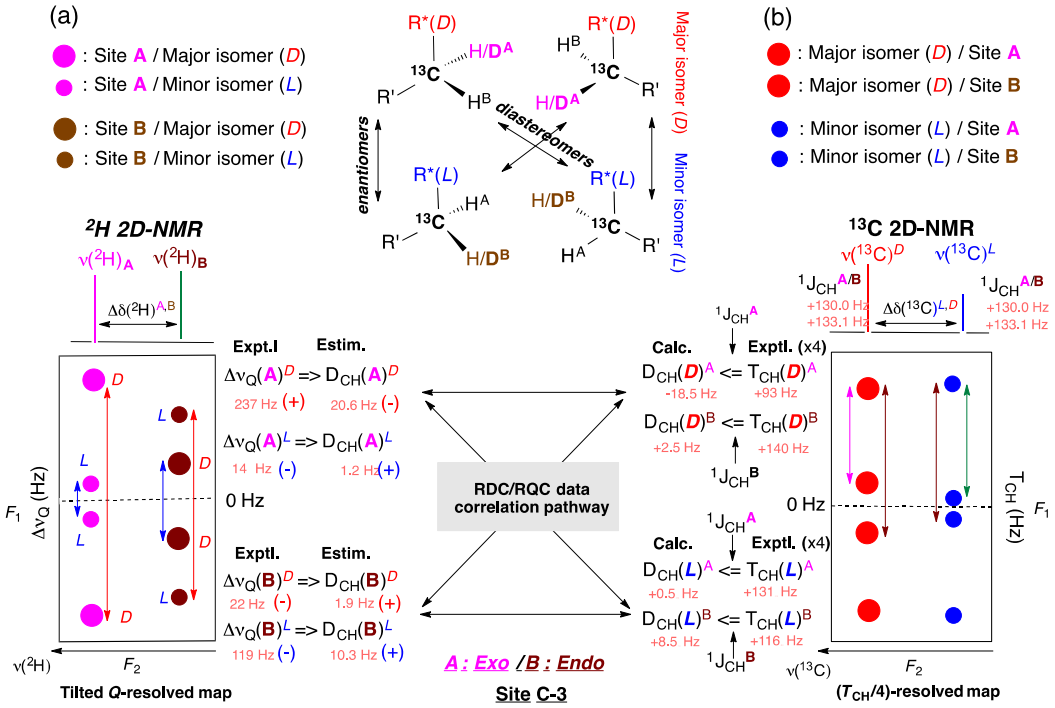

Figure SI-16. Analysis of the methylene group 3 of camphor along with the determination of the sign of ^{2}H-RQCs associated with the diastereotopic directions (*L*-MSP phase).

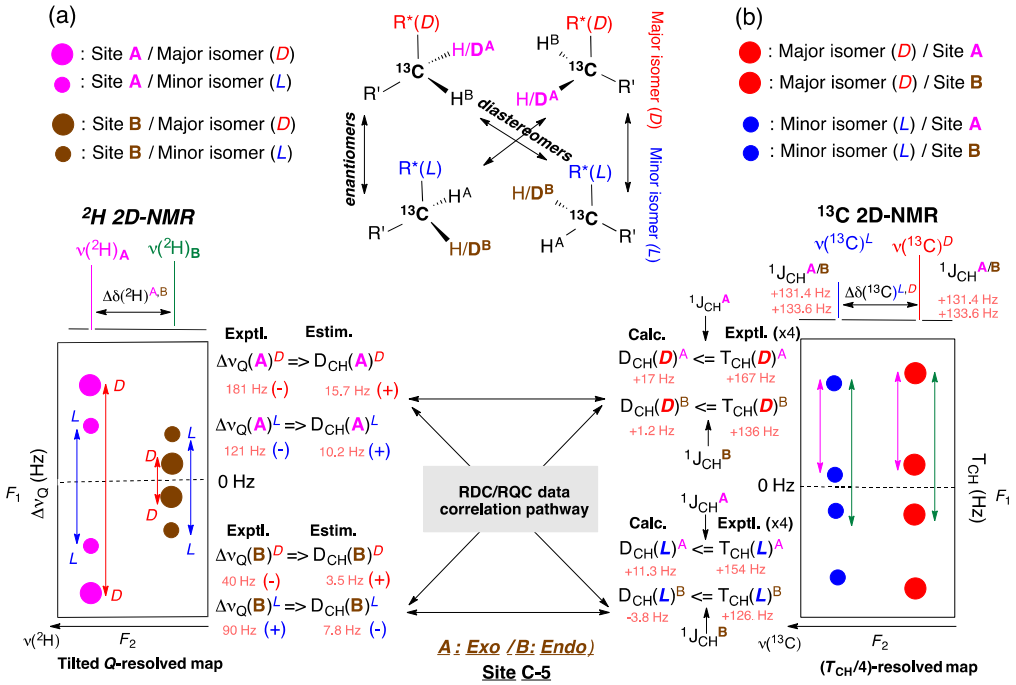

Figure SI-17. Analysis of the methylene group 5 of camphor along with the determination of the sign of ^{2}H-RQCs associated with the diastereotopic directions (*L*-MSP phase).

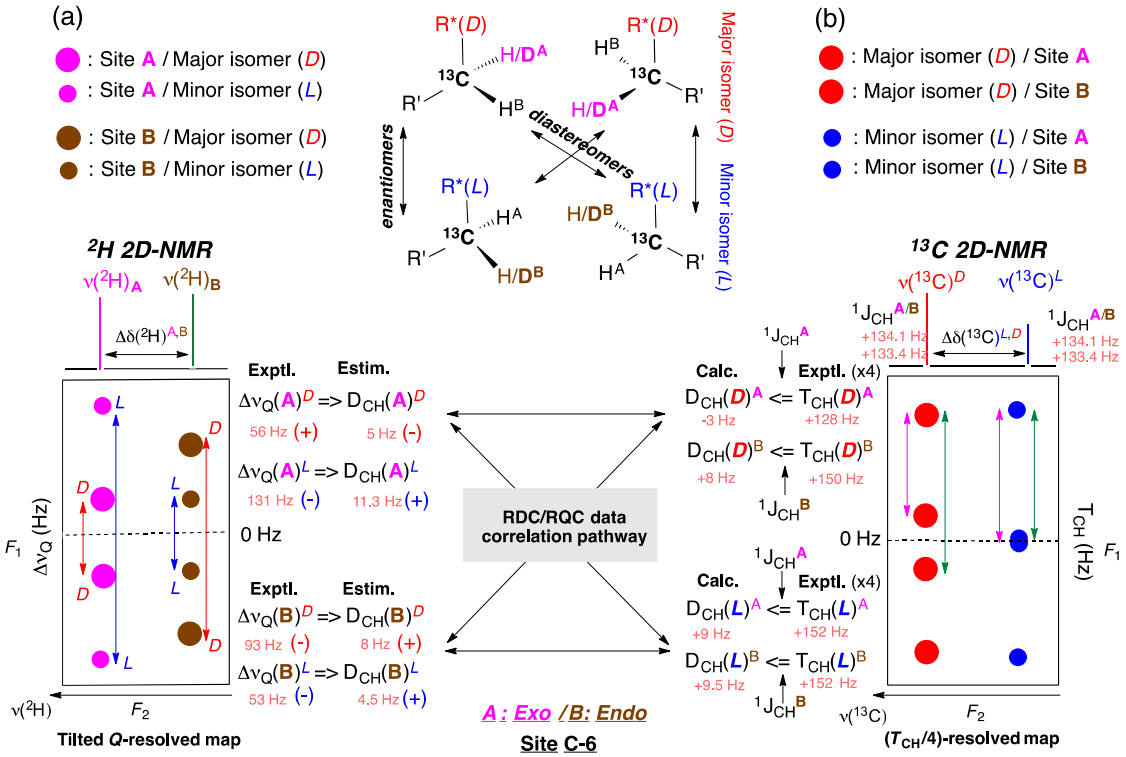

Figure SI-18. Analysis of the methylene group 6 of camphor along with the determination of the sign of ^{2}H-RQCs associated with the diastereotopic directions (*L*-MSP phase).

XI. Spectral data of (*D*)- and (*L*)-camphor in PDA/$CHCl_3$ (1)

Tables SI-5 and **SI-6** list all pertinent data of **5** in the PDA/$CHCl_3$ mesophase.

Table SI-5. ^2H and ^{13}C spectral data (ppm / Hz) of **5** dissolved in **PDA/$CHCl_3$**

$\Delta\nu_Q{}^2H$ ($CHCl_3$) = +92 Hz; Correction coefficient: $^1D_{CH}(CHCl_3)$@14T = -9.0 Hz // $^1D_{CH}$ ($CHCl_3$)@9.4T = -7.5 Hz => ratio = 1.20

^2H Spect. position [a]	10	9	8	7	6	5	4	3	2	1
Group	CH_2	CH	CH_2	CH_2	CH_2	CH_2	CH_2	CH_3	CH_3	CH_3
^2H Numbering	**3_{ex}**	**4**	**5_{ex}**	**3_{en}**	**6_{ex}**	**6_{en}**	**5_{en}**	**9**	**10**	**8**
$\delta(^1H)$ [b]	2.25	2.04	1.93	1.74	1.62	1.38	1.34	0.96	0.88	0.84
$\delta(^1H)^{Exptl.}$ ($CDCl_3$) [c]	2.34	2.08	1.94	1.83	1.67	1.38	1.34	0.95	0.90	0.82
$\delta(^2H)^{Exptl.}$ ($PBLG/CHCl_3$) [d]	**2.31**	**2.05**	**1.92**	**1.80**	**1.64**	**1.36**	**1.30**	**0.93**	**0.88**	**0.80**
^{13}C Numbering	**3**	**4**	**5**	**3**	**6**	**6**	**5**	**9**	**10**	**8**
$\delta(^{13}C)$ [e]	43.2	43.0	27.0	43.2	29.8	29.8	27.0	19.1	9.2	19.7
$\delta(^{13}C)^{Exptl.}$ ($CDCl_3$) [f]	43.3	43.0	27.0	43.3	29.9	29.9	27.1	19.1	9.2	19.7
$\delta(^{13}C)^{Exptl.}$ ($PDA/CHCl_3$) [g]	42.9	42.7	27.7	42.9	29.5	29.5	26.7	18.7	8.8	19.4
$^1J_{CH}$ ($CDCl_3$) [h]	+130.0	+142.7	+131.4	+133.1	+134.1	+133.4	+133.6	+125.1	+126.0	+124.9
$^1T_{CH}$ (*D*) [i]	≈+122	≈+140	≈+163	≈+122	≈+140	≈+142	≈+129	≈+116	≈+132	≈+128
$^1T_{CH}$ (*L*) [i]	≈+122	≈+140	≈+163	≈+122	≈+140	≈+142	≈+129	≈+116	≈+132	≈+128
$^1D_{CH}$ (*D*) [j]	-5	-2	+16	-5	+3	+4	-2	-4	+3	+2
$^1D_{CH}$ (*L*) [j]	-5	-2	+16	-5	+3	+4	-2	-4	+3	+2
Sign of $^1D_{CH}$ (*D*)	< 0	< 0	> 0	< 0	> 0	> 0	< 0	< 0	> 0	> 0
Sign of $^1D_{CH}$ (*L*)	< 0	< 0	> 0	< 0	> 0	> 0	< 0	< 0	> 0	> 0
Sign of $\Delta\nu_Q(^2H)$ (*D*)	> 0	> 0	< 0	> 0	< 0	< 0	> 0	> 0	< 0	< 0
Sign of $\Delta\nu_Q(^2H)$ (*L*)	> 0	> 0	< 0	> 0	< 0	< 0	> 0	> 0	< 0	< 0
$\Delta\nu_Q^{Exptl.}$ (*D*) [k]	**+75 ± 1**	**+5 ± 1**	**-197 ± 1**	**+42± 1**	**-35 ± 1**	**-79 ± 1**	**+30 ± 1**	**+50 ± 1**	**-33 ± 1**	**-23 ± 1**
$\Delta\nu_Q^{Exptl.}$ (*L*) [k]	**+75 ± 1**	**+26 ± 1**	**-197 ± 1**	**+50 ± 1**	**-47 ± 1**	**-111 ± 1**	**+38 ± 1**	**+54 ± 1**	**-37 ± 1**	**-28 ± 1**
$^1D_{CH}^{Estim.}$ (*D*) [l]	-6.5	< 1	+17.1	-3.6	+2.9	+6.8	-2.6	-4.3	+2.9	+2
$^1D_{CH}^{Estim.}$ (*L*) [l]	-6.5	-2.3	+17.1	-4.4	+4.1	+9.5	-3.3	-4.7	+3.2	+2.4

[a] ^2H NMR data ranked from the most deshielded ^2H site (Pos. 10) to the most shielded one (Pos. 1) (see the associated tilted NAD 2D spectrum). [b] Data (in ppm) from Kaiser's article (*Magn. Reson. Chem., 1994, (32), 503*). [c] The experimental $\delta(^1H)^{iso}$ values -ppm- measured with our conditions with $\delta(CDCl_3)$ = 7.27 ppm. [d] The $\delta(^2H)^{aniso}$ values -ppm- measured in the **PDA** mesophase (from the tilted NAD-{^1H} *Q*-resolved Fz 2D map) with $\delta(CHCl_3)$ = 7.27 ppm). [e] Data (in ppm) from Crull's article (*Magn. Reson. Chem., 1986, (24), 737).* [f] The experimental $\delta(^{13}C)^{iso}$ values -ppm- measured with $\delta(CHCl_3)$ = 77.0 ppm. [g] The $\delta(^{13}C)^{aniso}$ values (in ppm) measured in the **PDA** phase, with $\delta(CHCl_3)$ = 77.0 ppm. [h] $^1J_{CH}$ values (in Hz) extracted from the CLIP-HSQC 2D experiment. [i] Approximate $^1T_{CH}$ values evaluated from anisotropic ^{13}C-^1H spectra (1D and/or 2D T_{CH}-resolved experiments). [j] $^1D_{CH}$ (Hz) = [$^1T_{CH}$ - $^1J_{CH}$]/2. [k] Experimental ^2H-RQC values (in ppm) extracted from the ANAD-{^1H} *Q*-resolved Fz 2D spectrum. [l] Estimated $^1D_{CH}$ values (Hz) calculated using the relationship: $^1D_{CH}{}^{Estimated} \approx -\Delta\nu_Q{}^{Exptl}/11.5$.

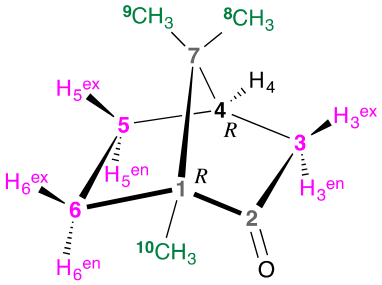

D-camphor (**(*D*)-5**)

Table SI-6. Comparison between ^{2}H-RQC$^{Exptl.}$ and ^{2}H-RQC$^{Calc.}$ of **5** dissolved in **PDA/CHCl$_3$**
Q(*D*) value = 0 .06558 // Q(*L*) value = 0.04168

^{2}H Spect. Position [a]	**10**	**9**	**8**	**7**	**6**	**5**	**4**	**3**	**2**	**1**
Group	CH_2	CH	CH_2	CH_2	CH_2	CH_2	CH_2	CH_3	CH_3	CH_3
^{2}H Numbering	**3$_{ex}$**	**4**	**5$_{ex}$**	**3$_{en}$**	**6$_{ex}$**	**6$_{en}$**	**5$_{en}$**	**9**	**10**	**8**
$\Delta\nu_Q^{Exptl.}$ (*D*) / Hz [b]	**+75 ± 1**	**+5 ± 1**	**-197 ± 1**	**+42± 1**	**-35 ± 1**	**-79 ± 1**	**+30 ± 1**	**+50 ± 1**	**-33 ± 1**	**-23 ± 1**
$\Delta\nu_Q^{Calc.}$ (*D*) / Hz [c]	**+80.7**	**+13.9**	**-189.9**	**+45.4**	**-34.6**	**-82.1**	**+37.3**	**+50.9**	**-31.7**	**-26.5**
$\Delta\Delta\nu_Q$ / Hz [d]	+5.7	+8.9	+7.1	+3.4	+0.4	-3.1	+7.3	+0.9	+1.4	-3.5
Rel. □□□□. (%) [e]	7.1	64.1	3.7	7.4	1.1	3.8	19.6	1.7	4.3	13.2
$\Delta\nu_Q^{Exptl.}$ (*L*) / Hz [b]	**+75 ± 1**	**+26 ± 1**	**-197 ± 1**	**+50 ± 1**	**-47 ± 1**	**-111 ± 1**	**+38 ± 1**	**+54 ± 1**	**-37 ± 1**	**-28 ± 1**
$\Delta\nu_Q^{Calc.}$ (*L*) / Hz [c]	**+72.4**	**+20.1**	**-200.0**	**+44.5**	**-47.2**	**-107.9**	**+37.1**	**+57.3**	**-40.9**	**-26.5**
$\Delta\Delta\nu_Q$ / Hz [d]	-2.6	-5.9	-3.0	-5.5	-0.2	+3.1	-0.9	+3.3	-3.9	+1.5
Rel. D□□□. (%) [e]	3.6	29.5	1.5	12.2	0.3	2.9	2.3	5.8	9.6	5.6

[a] ^{2}H NMR data ranked from the most deshielded ^{2}H site (Pos. 10) to the most shielded one (Pos. 1) (see the associated tilted NAD 2D spectrum). [b] Experimental ^{2}H-RQC values extracted from ANAD-{^{1}H} *Q*-resolved-Fz 2D spectrum. [c] Back-calculated ^{2}H-RQC values calculated (best SVD-fit) using ConArch$^+$ program. [d] $\Delta\Delta\nu_Q$ (Hz) = $\Delta\nu_Q^{Calc.}(D)$ - $\Delta\nu_Q^{Exptl.}(D)$. [e] Relative difference: Rel. Diff. (%) = $|\Delta\nu_Q^{Calc.}(D) - \Delta\nu_Q^{Exptl.}(D)| / |\Delta\nu_Q^{Calc.}(D)|$.

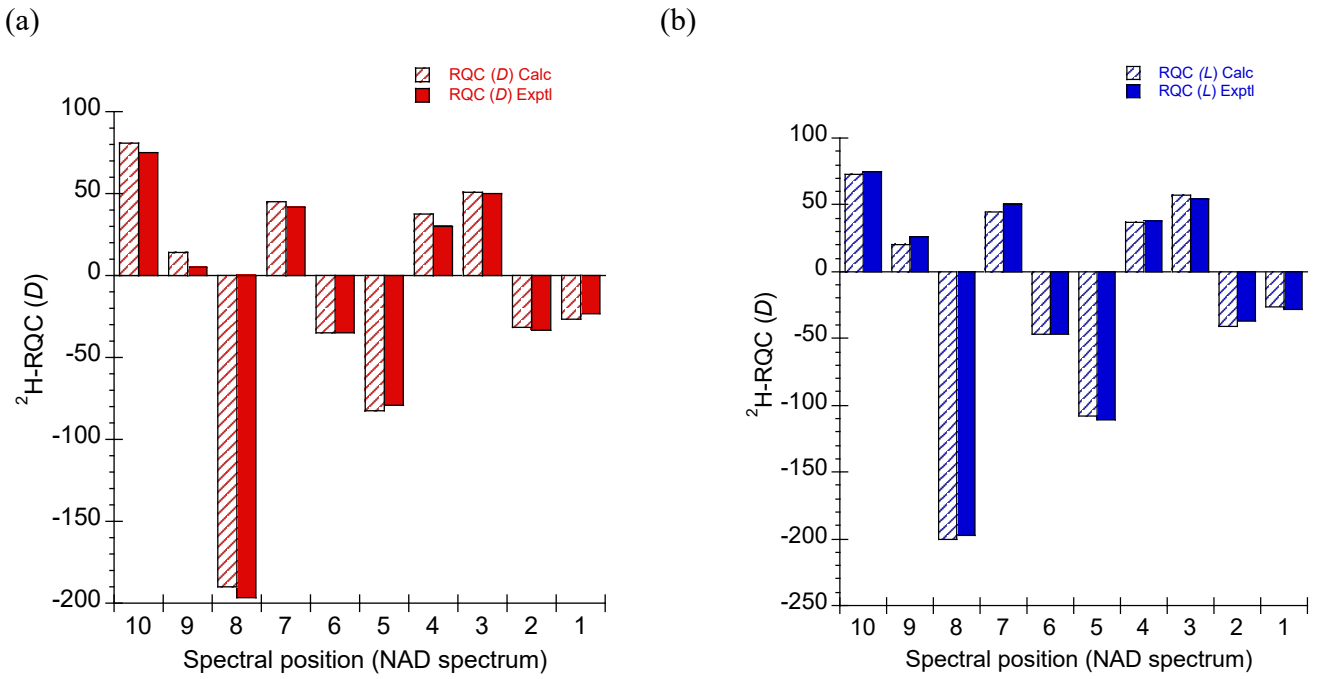

Figure SI-19. Comparison between ^{2}H-RQC^{Exptl} and ^{2}H-RQC^{Calc} values *versus* the position ^{2}H-DQs on the NAD F_2 projection of the *Q*-resolved map of **5** (see **Figure 3a**) dissolved in the PDA mesophase: (a) (*D*)-enantiomer, (b) (*L*)-enantiomer.

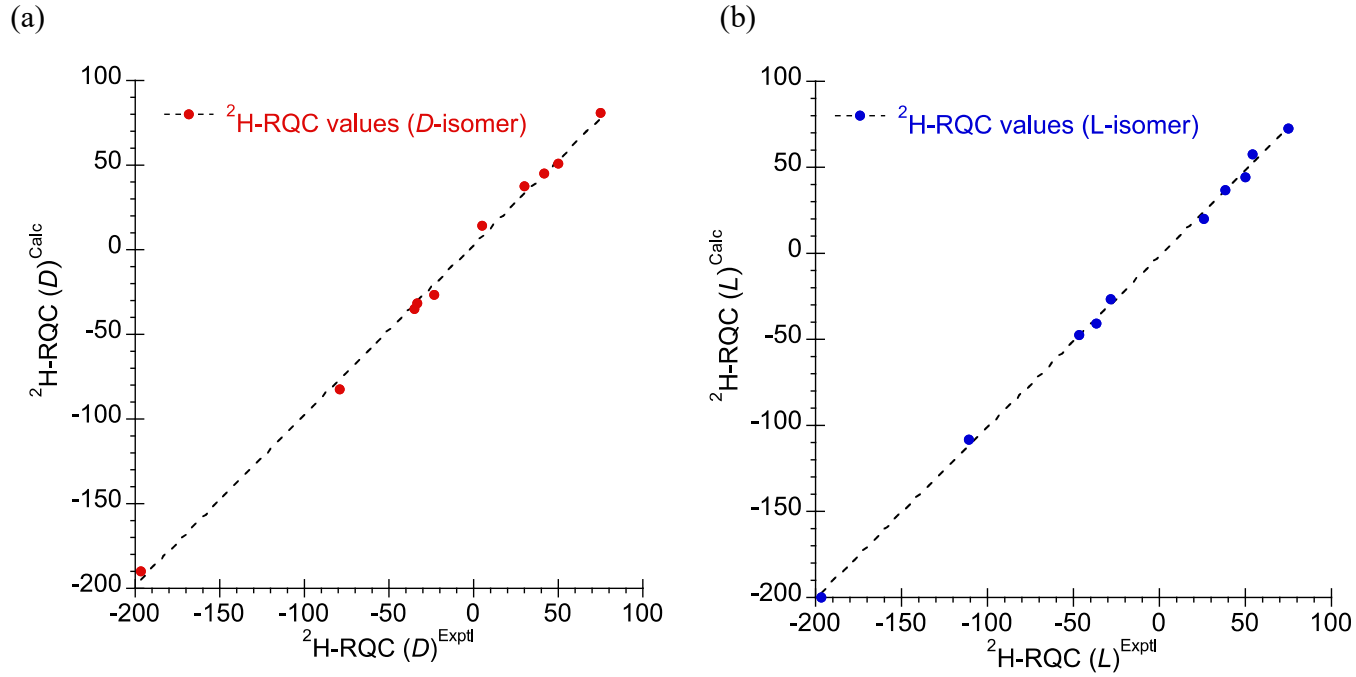

Figure SI-20. Correlation plots (^{2}H-RQC$^{Calc.}$ *versus* ^{2}H-RQC$^{Exptl.}$) of **5** dissolved in the PDA mesophase obtained for the best-fit data/structure: (a) for the (*D*)-enantiomer, (b) (*L*)-enantiomer. The *Q*-factor obtained is equal to 0.0656 and 0.0417, respectively.

XII. Spectral data of (*D*)- and (*L*)-camphor in *L*-MSP/$CHCl_3$ (2)

Tables SI-7 and **SI-8** list all pertinent data of **5** in the L-MSP/$CHCl_3$ mesophase.

Table SI-7. ^2H and ^{13}C spectral data (ppm / Hz) of **5** dissolved in ***L*-MSP/$CHCl_3$**
$\Delta\nu_Q$ ^2H ($CHCl_3$) = +771 Hz; Correction coefficient: $^1D_{CH}$($CHCl_3$)@14T = -71.5 Hz // $^1D_{CH}$ ($CHCl_3$)@9.4T = -76 Hz => ratio = 1.06

^2H Spect. position [a]	10	9	8	7	6	5	4	3	2	1
Group	CH_2	CH	CH_2	CH_2	CH_2	CH_2	CH_2	CH_3	CH_3	CH_3
^2H Numbering	**3_{ex}**	**4**	**5_{ex}**	**3_{en}**	**6_{ex}**	**6_{en}**	**5_{en}**	**9**	**10**	**8**
$\delta(^1H)$ [b]	2.25	2.04	1.930	1.74	1.62	1.38	1.34	0.96	0.88	0.84
$\delta(^1H)^{Exptl.}$ ($CDCl_3$) [c]	2.34	2.08	1.94	1.83	1.67	1.38	1.34	0.95	0.90	0.82
$\delta(^2H)^{Exptl.}$ (*PBLG/$CHCl_3$*) [d]	**2.31**	**2.06**	**1.91**	**1.80**	**1.64**	**1.38**	**1.30**	**0.93**	**0.88**	**0.80**
^{13}C Numbering	3	4	5	3	6	6	5	9	10	8
$\delta(^{13}C)$ [e]	43.2	43.0	27.0	43.2	29.8	29.8	27.0	19.1	9.2	19.7
$\delta(^{13}C)^{Exptl.}$ ($CDCl_3$) [f]	43.3	43.0	27.0	43.3	29.9	29.9	27.1	19.1	9.2	19.7
$\delta(^{13}C)^{Exptl.}$ (*L-MSP/$CHCl_3$*) [g]	42.8	42.6	26.6	42.8	29.5	29.5	26.6	18.7	8.8	19.3
$^1J_{CH}$ (>0) ($CDCl_3$) [h]	+130.0	+142.7	+131.4	+133.1	+134.1	+133.4	+133.6	+125.1	+126.0	+124.9
$^1T_{CH}$ (*D*) [i]	≈+93	≈+151	≈+159	≈+147	≈+128	≈+153	≈+126	≈+118	≈+128	≈+132
$^1T_{CH}$ (*L*) [i]	≈+140	≈+151	≈+159	≈+116	≈+150	≈+153	≈+126	≈+118	≈+121	≈+132
$^1D_{CH}$ (*D*) [j]	-18.5	+4	+14	+2.5	-3	+10	-4	-3.5	+1	+3.5
$^1D_{CH}$ [f] (*L*) [j]	+0.5	+4	+14	-8.5	+8	+10	-4	-3.5	+2	+3.5
Sign of $^1D_{CH}$ (*D*)	< 0	> 0	> 0	> 0	<0	> 0	< 0	< 0	> 0	> 0
Sign of $^1D_{CH}$ (*L*)	> 0	> 0	> 0	< 0	> 0	> 0	< 0	< 0	> 0	> 0
Sign of $\Delta\nu_Q(^2H)$ (*D*)	> 0	< 0	< 0	< 0	> 0	< 0	> 0	> 0	< 0	< 0
Sign of $\Delta\nu_Q(^2H)$ (*L*)	< 0	< 0	< 0	> 0	< 0	< 0	> 0	> 0	< 0	< 0
$\Delta\nu_Q^{Exptl.}$ (*D*) [k]	**+237 ± 1**	**-62 ± 1**	**-181 ± 1**	**-22 ± 1**	**+56 ± 1**	**-93 ± 1**	**-40 ± 1**	**+41 ± 1**	**+6 ± 1**	**-52 ± 1**
$\Delta\nu_Q^{Exptl.}$ (*L*) [k]	**-14 ± 1**	**-30 ± 1**	**-121 ± 1**	**+119 ± 1**	**-131 ± 1**	**-53 ± 1**	**+90 ± 1**	**+48 ± 1**	**-19 ± 1**	**-39 ± 1**
$^1D_{CH}^{Estim.}$ (*D*) [l]	-20.6	+5.4	+15.7	1.9	-4.9	+8.0	-3.5	-3.6	<1	+4.5
$^1D_{CH}^{Estim.}$ (*L*) [l]	+1.2	+2.6	+10.2	-10.3	+11.4	+4.6	-7.8	-4.2	+1.7	+3.4

[a] ^2H NMR data ranked from the most deshielded ^2H site (Pos. 10) to the most shielded one (Pos. 1) (see the associated tilted NAD 2D spectrum). [b] Data (in ppm) from Kaiser's article (*Magn. Reson. Chem., 1994, (32), 503*). [c] The experimental $\delta(^1H)^{iso}$ values (in ppm) measured with our conditions with $\delta(CDCl_3)$ = 7.27 ppm. [d] The $\delta(^2H)^{aniso}$ values (in ppm) measured in the L-MSP mesophase (from the tilted NAD-{^1H} *Q*-resolved Fz 2D map) with $\delta(CDCl_3)$ = 7.27 ppm). [e] Data (in ppm) from Crull's article (*Magn. Reson. Chem., 1986, (24), 737).* [f] The experimental $\delta(^{13}C)^{iso}$ values -ppm- measured with our conditions, with $\delta(CHCl_3)$ = 77.0 ppm. [g] The $\delta(^{13}C)^{aniso}$ values -ppm- measured in the L-MSP phase, with $\delta(CHCl_3)$ = 77.0 ppm. [h] $^1J_{CH}$ values (in Hz) extracted from the CLIP-HSQC 2D experiment. [i] Approximate $^1T_{CH}$ values evaluated from anisotropic ^{13}C-^1H spectra (1D and/or 2D T_{CH}-resolved experiments). [j] $^1D_{CH}$ (Hz) = [$^1T_{CH}$ - $^1J_{CH}$]/2. [k] Experimental ^2H-RQC values (Hz) extracted from the ANAD-{^1H} *Q*-resolved Fz 2D spectrum. [l] Estimated $^1D_{CH}$ values (Hz) calculated using the relationship: $^1D_{CH}^{Estimated} \approx -\Delta\nu_Q^{Exptl.}/11.5$.

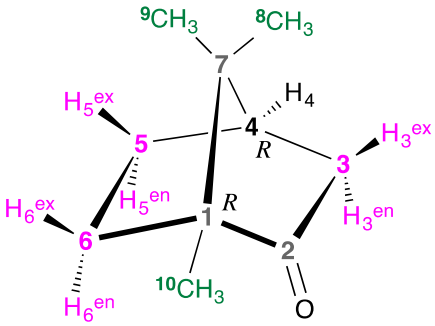

D-camphor (**(*D*)-5**)

Table SI-8. Comparison between ^{2}H-RQC^{Exptl} and ^{2}H-RQC^{Calc} of **5** dissolved in ***L*-MSP/CHCl$_3$**
Q(*D*) value = 0 .060618 // Q(*L*) value = 0.06030

^{2}H Spect. Position [a]	**10**	**9**	**8**	**7**	**6**	**5**	**4**	**3**	**2**	**1**
Group	CH_2	CH	CH_2	CH_2	CH_2	CH_2	CH_2	CH_3	CH_3	CH_3
^{2}H Numbering	**3_{ex}**	**4**	**5_{ex}**	**3_{en}**	**6_{ex}**	**6_{en}**	**5_{en}**	**9**	**10**	**8**
$\Delta\nu_Q^{Exptl.}$ (*D*) / Hz [b]	**+237 ± 1**	**-62 ± 1**	**-181 ± 1**	**-22 ± 1**	**+56 ± 1**	**-93 ± 1**	**-40 ± 1**	**+41 ± 1**	**+6 ± 1**	**-52 ± 1**
$\Delta\nu_Q^{Calc.}$ (*D*) / Hz [c]	**+244.0**	**-50.3**	**-172.2**	**-16.1**	**+56.7**	**-97.1**	**-32.4**	**+40.1**	**+7.1**	**-57.8**
$\Delta\Delta\nu_Q$ / Hz [d]	+7.0	+11.7	+8.8	+5.9	+0.7	-4.1	+7.7	-0.9	+1.1	-5.8
Rel. □□□□. (%) [e]	2.9	23.2	5.1	36.9	1.2	4.2	23.6	2.3	15.0	10.0
$\Delta\nu_Q^{Exptl.}$ (*L*) / Hz [b]	**-14 ± 1**	**-30 ± 1**	**-121 ± 1**	**+119 ± 1**	**-131 ± 1**	**-53 ± 1**	**+90 ± 1**	**+48 ± 1**	**-19 ± 1**	**-39 ± 1**
$\Delta\nu_Q^{Calc.}$ (*L*) / Hz [c]	**-12.6**	**-36.0**	**-122.9**	**113.3**	**-133.6**	**-50.1**	**91.1**	**47.1**	**-26.9**	**-30.5**
$\Delta\Delta\nu_Q$ / Hz [d]	1.4	-6.0	-1.9	-5.7	-2.6	+3.0	+1.1	-1.0	-7.9	+8.5
Rel. D□□□. (%) [e]	10.8	16.6	1.6	5.1	2.0	5.9	1.2	2.0	29.4	27.7

[a] ^{2}H NMR data ranked from the most deshielded ^{2}H site (Pos. 10) to the most shielded one (Pos. 10) to the most shielded one (Pos. 1) (see the associated tilted NAD 2D spectrum. [b] Experimental ^{2}H-RQC values extracted from ANAD-{^{1}H} *Q*-resolved-Fz 2D spectrum. [c] Back-calculated ^{2}H-RQCs calculated (best SVD-fit) using ConArch$^+$ program. [d] $\Delta\Delta\nu_Q = \Delta\nu_Q^{Calc.}(D) - \Delta\nu_Q^{Exptl.}(D)$. [e] Relative difference: Rel. Diff. (%) = $|\Delta\nu_Q^{Calc.}(D) - \Delta\nu_Q^{Exptl.}(D)| / |\Delta\nu_Q^{Calc.}(D)|$.

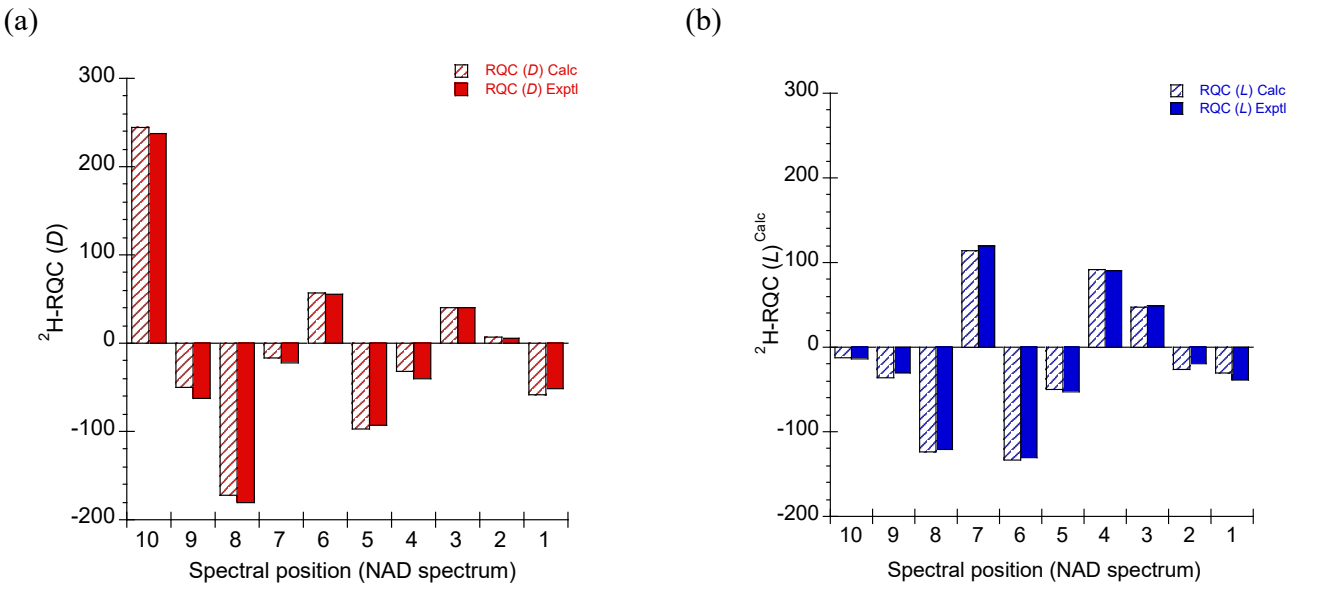

Figure SI-21. Comparison between ^{2}H-RQC$^{Exptl.}$ and ^{2}H-RQC$^{Calc.}$ values *versus* the position ^{2}H-DQs on the NAD F_2 projection of the *Q*-resolved map of **5** (see **Figure 2b**) dissolved in the *L*-MSP mesophase: (a) (*D*)-enantiomer, (b) (*L*)-enantiomer.

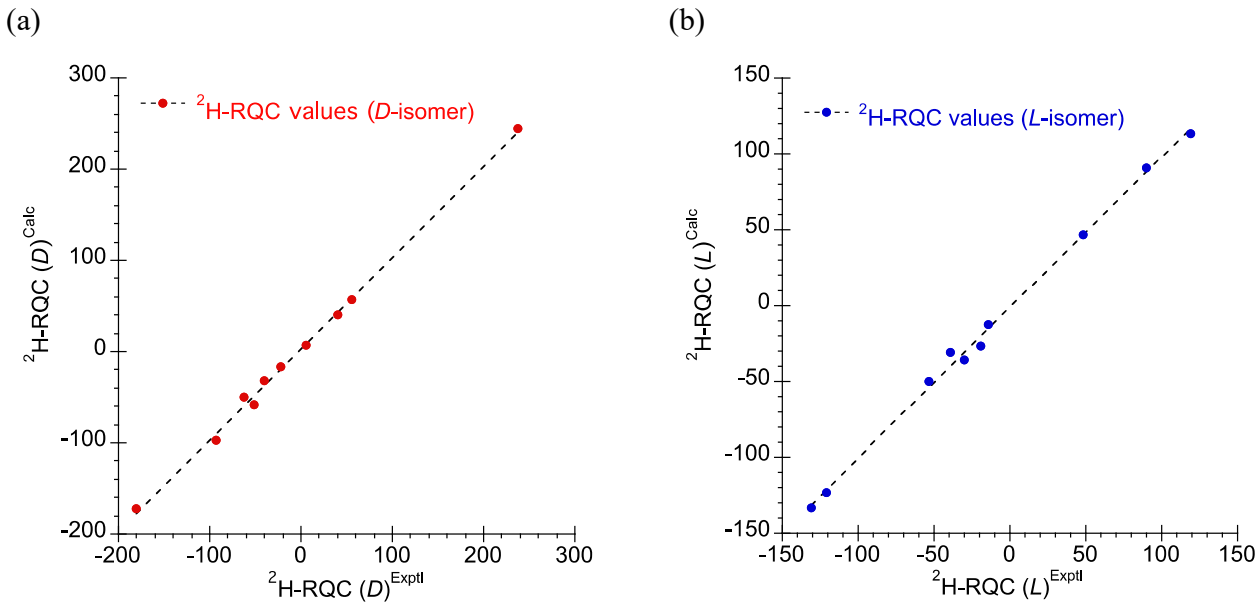

Figure SI-22. Correlation plots (^{2}H-RQC$^{Calc.}$ *versus* ^{2}H-RQC$^{Exptl.}$) of **5** dissolved in the L-MSP mesophase obtained for the best-fit data/structure: (a) (*D*)-enantiomer, (b) (*L*)-enantiomer. The *Q*-factor obtained is equal to 0.0606 and 0.0603, respectively.

XIII. Spectral data of (*D*)- and (*L*)-camphor oriented in PBLG/$CHCl_3$ (3)

Tables SI-9 and **SI-10** list all pertinent data of **5** in the PBLG/$CHCl_3$ mesophase.

Table SI-9. ^2H and ^{13}C spectral data (ppm / Hz) of **5** dissolved in **PBLG/$CHCl_3$**
$\Delta\nu_Q$ ^2H ($CHCl_3$)@14T = +864 Hz; Correction coefficient: **$^1D_{CH}$($CHCl_3$)@14T = -78.5 Hz // $^1D_{CH}$ ($CHCl_3$)@9.4T = -77.5 Hz /=> ratio = 1.01**

^2H Spect. position [a]	**10**	**9**	**8**	**7**	**6**	**5**	**4**	**3**	**2**	**1**
Group	CH_2	CH	CH_2	CH_2	CH_2	CH_2	CH_2	CH_3	CH_3	CH_3
^2H Numbering	**3_{ex}**	**4**	**5_{ex}**	**3_{en}**	**6_{ex}**	**6_{en}**	**5_{en}**	**9**	**10**	**8**
$\delta(^1H)$ [b]	2.25	2.04	1.93	1.74	1.62	1.38	1.34	0.96	0.88	0.84
$\delta(^1H)^{Exptl.}$ ($CDCl_3$) [c]	2.34	2.08	1.94	1.83	1.67	1.38	1.34	0.95	0.90	0.82
$\delta(^2H)^{Exptl.}$ ($PBLG/CHCl_3$) [d]	**2.33**	**2.07**	**1.93**	**1.82**	**1.67**	**1.38**	**1.32**	**0.94**	**0.90**	**0.82**
^{13}C Numbering	**3**	**4**	**5**	**3**	**6**	**6**	**5**	**9**	**10**	**8**
$\delta(^{13}C)$ [e]	43.2	43.0	27.0	43.2	29.8	29.8	27.0	19.1	9.2	19.7
$\delta(^{13}C)^{Exptl.}$ ($CDCl_3$) [f]	43.3	43.0	27.0	43.3	29.9	29.9	27.1	19.1	9.2	19.7
$\delta(^{13}C)^{Exptl.}$ ($PBLG/CHCl_3$) [g]	42.9	42.8	26.8	42.9	29.7	29.7	26.8	18.7	9.0	19.5
$^1J_{CH}$ ($CDCl_3$) [h]	+130.0	+142.7	+131.4	+133.1	+134.1	+133.4	+133.6	+125.1	+126.0	+124.9
$^1T_{CH}$ (*D*) [i]	≈+226	≈+153	≈-25	≈+150	≈+114	≈+38	≈+147	≈+169	≈+98	≈+102
$^1T_{CH}$ (*L*) [i]	≈+226	≈+153	≈-25	≈+150	≈-114	≈+38	≈+147	≈+169	≈+98	≈+102
$^1D_{CH}$ (*D*) [j]	+48	+5	-78	+11	-10	-47	+7	+22	-14	-12
$^1D_{CH}$ [f] (*L*) [j]	+48	+5	-78	+11	-10	-47	+7	+22	-14	-12
Sign of $^1D_{CH}$ (*D*)	> 0	> 0	< 0	> 0	< 0	< 0	> 0	> 0	<0	<0
Sign of $^1D_{CH}$ (*L*)	> 0	> 0	< 0	> 0	< 0	< 0	> 0	> 0	< 0	<0
Sign of $\Delta\nu_Q(^2H)$ (*D*)	< 0	< 0	> 0	< 0	> 0	> 0	< 0	< 0	> 0	< 0
Sign of $\Delta\nu_Q(^2H)$ (*L*)	< 0	< 0	> 0	< 0	> 0	> 0	< 0	< 0	> 0	> 0
$\Delta\nu_Q^{Exptl.}$ (*D*) [k]	**-546 ± 1**	**-40 ± 1**	**+1080 ± 1**	**-182 ± 1**	**+88 ± 1**	**+598 ± 1**	**-129 ± 1**	**-283 ± 1**	**+174 ± 1**	**+155 ± 1**
$\Delta\nu_Q^{Exptl.}$ (*L*) [k]	**-598 ± 1**	**-18 ± 1**	**+1044 ±1**	**-141 ± 1**	**+102 ± 1**	**+626 ± 1**	**-77 ± 1**	**-283 ± 1**	**+160 ± 1**	**+176 ± 1**
$^1D_{CH}^{Estim.}$ (*D*) [l]	+47.4	+3.5	-93.9	+15.8	-7.3	-51.7	+11.2	+24.6	-15.0	-13.4
$^1D_{CH}^{Estim.}$ (*L*) [l]	+52.0	+1.5	90.8	+12.2	-8.8	-54.2	+6.3	+24.6	-13.9	-15.3

[a] ^2H NMR data ranked from the most deshielded ^2H site (Pos. 10) to the most shielded one (Pos. 1) (see the associated tilted NAD 2D spectrum). [b] Data (in ppm) from Kaiser's article (*Magn. Reson. Chem., 1994, (32), 503*). [c] The experimental $\delta(^1H)^{iso}$ values (in ppm) measured with our conditions with $\delta(CDCl_3)$ = 7.27 ppm. [d] The $\delta(^2H)^{aniso}$ values -ppm- measured in the PBLG mesophase (from the tilted NAD-{^1H} *Q*-resolved Fz 2D map) with $\delta(CHCl_3)$ = 7.27 ppm). [e] Data (in ppm) from Crull's article (*Magn. Reson. Chem., 1986, (24), 737).* [f] The experimental $\delta(^{13}C)^{iso}$ values (in ppm) measured with our conditions with $\delta(CHCl_3)$ = 77.0 ppm. [g] The $\delta(^{13}C)^{aniso}$ values (in ppm) measured in the PBLG phase, with $\delta(CHCl_3)$ = 77.0 ppm. [h] $^1J_{CH}$ values (in Hz) extracted from the CLIP-HSQC 2D experiment. [i] Approximate $^1T_{CH}$ values evaluated from anisotropic ^{13}C-^1H spectra (1D and/or 2D T_{CH}-resolved experiments). [j] $^1D_{CH}$ = [$^1T_{CH}$ - $^1J_{CH}$]/2. [k] Experimental ^2H-RQC values (in Hz) extracted from the ANAD-{^1H} *Q*-resolved Fz 2D spectrum. [l] Estimated $^1D_{CH}$ values (in Hz) calculated using the relationship: $^1D_{CH}^{Estimated} \approx -\Delta\nu_Q^{Exptl}/11.5$.

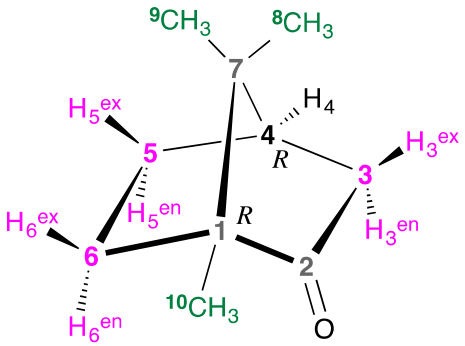

D-camphor (**(*D*)-5**)

Table SI-10. Comparision between ^{2}H-RQC^{Exptl} and ^{2}H-RQC^{Calc} of (*D*) -and (*L*)-**5** dissolved in **PBLG/CHCl$_3$** Q(*D*) value = 0.01708 // Q(*L*) value = 0.01725

^{2}H Spect. Position [a]	**10**	**9**	**8**	**7**	**6**	**5**	**4**	**3**	**2**	**1**
Group	CH_2	CH	CH_2	CH_2	CH_2	CH_2	CH_2	CH_3	CH_3	CH_3
Num. ^{2}H	**3$_{ex}$**	**4**	**5$_{ex}$**	**3$_{en}$**	**6$_{ex}$**	**6$_{en}$**	**5$_{en}$**	**9**	**10**	**8**
$\Delta\nu_Q^{Exptl.}$ (*D*) / Hz [b]	**-546.0**	**-40.0**	**+1080.0**	**-182.0**	**+88.0**	**+598.0**	**-129.0**	**-283.0**	**+174.0**	**+155.0**
$\Delta\nu_Q^{Calc.}$ (*D*) / Hz [c]	**-554.2**	**-46.1**	**+1071.3**	**-176.4**	**89.0**	**+597.4**	**-144.0**	**-286.0**	**+184.9**	**+159.6**
$\Delta\Delta\nu_Q$ / Hz [d]	-8.2	-6.1	-8.7	+5.7	+1.0	-0.6	-15.0	-3.0	+10.9	+4.6
Rel. □□□□. (%) [e]	1.5	13.3	0.8	+3.2	1.1	0.1	10.4	1.0	5.9	2.9
$\Delta\nu_Q^{Exptl.}$ (*L*) / Hz [b]	**-598.0**	**-18.0**	**+1044.0**	**-141.0**	**+102.0**	**+626.0**	**-77.0**	**-283.0**	**+160.0**	**+176 ± 1**
$\Delta\nu_Q^{Calc.}$ (*L*) / Hz [c]	**-606.5**	**-23.5**	**+1035.0**	**-135.4**	**+102.9**	**+625.0**	**-91.7**	**-288.2**	**+171.6**	**+178.5**
$\Delta\Delta\nu_Q$ / Hz [d]	-8.5	-5.5	-9.0	+5.6	+0.9	-1.0	-14.7	-5.2	+11.6	+2.5
Rel. D□□□. (%) [e]	1.4	23.2	0.9	4.1	0.9	0.2	16.0	1.8	6.8	1.40

[a] ^{2}H NMR data ranked from the most deshielded ^{2}H site (Pos. 10) to the most shielded one (Pos. 1) (see the associated tilted NAD 2D spectrum. [b] Experimental ^{2}H-RQC values extracted from ANAD-{^{1}H} *Q*-resolved-Fz 2D spectrum. [c] Back-calculated ^{2}H-RQCs calculated (best SVD-fit) using ConArch$^+$ program. [d] $\Delta\Delta\nu_Q = \Delta\nu_Q^{Calc.}(D) - \Delta\nu_Q^{Exptl.}(D)$. [e] Relative difference: Rel. Diff. (%) = $|\Delta\nu_Q^{Calc.}(D) - \Delta\nu_Q^{Exptl.}(D)| / |\Delta\nu_Q^{Calc.}(D)|$.

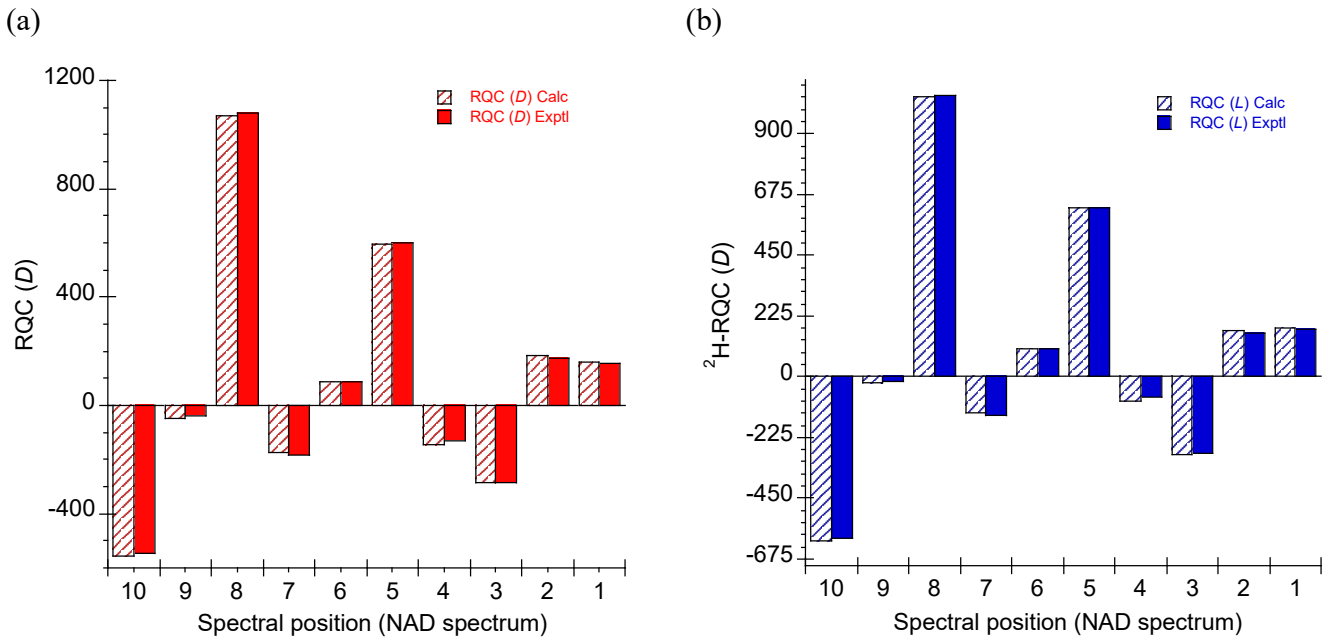

Figure SI-23. Comparison between ^{2}H-RQC$^{\text{Exptl.}}$ and ^{2}H-RQC$^{\text{Calc.}}$ values *versus* the position ^{2}H-DQs on the NAD F_2 projection of camphor **5** (see **Figure SI-14**) dissolved in the PBLG mesophase: (a) for the (*D*)-enantiomer, (b) for the (*L*)-enantiomer.

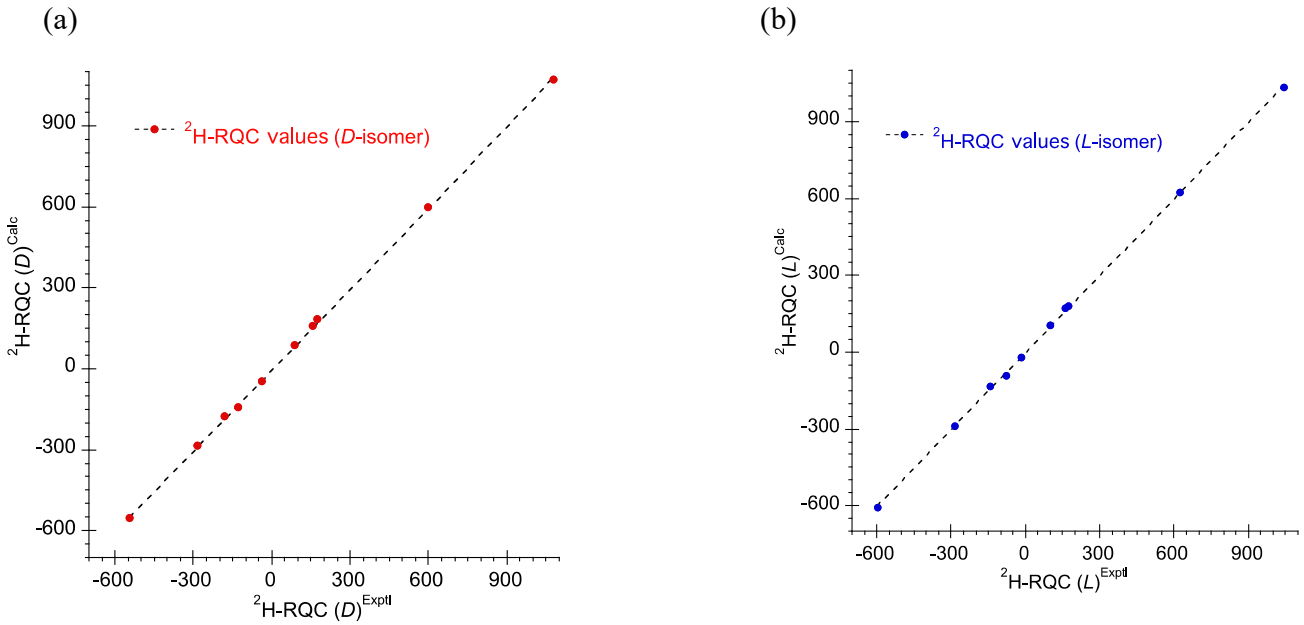

Figure SI-24. Correlation plot of back-calculated *vs*. experimental dataset (^{2}H-RQC$^{\text{Calc.}}$ *vs.* ^{2}H-RQC$^{\text{Exptl.}}$) of **5** dissolved in the PBLG mesophase obtained for the best-fit data/structure: (a) for the (*D*)-enantiomer, (b) for the (*L*)-enantiomer. The *Q*-factor obtained is equal to 0.0171 and 0.0173, respectively.

XIV. Spectral data of (*D*)- and (*L*)-camphor oriented in the PCBLL/DMF (4)

Tables SI-11 and **SI-12** list all pertinent data of **5** in the PCBLL/DMF mesophase.

Table SI-11. ^{2}H and ^{13}C spectral data (ppm / Hz) of **5** dissolved in **PCBLL/DMF**
$\Delta\nu_Q$ ^{2}H (DMF)@14T = +88, +155, +54 Hz; Correction coefficient: $^{1}D_{CH}$(DMF)@14T = -211 Hz / $^{1}D_{CH}$ (DMF)@9.4T = -211 Hz /=> ratio = 1.00

^{2}H Spect. position [a]	10	9	8	7	6	5	4	3	2	1
Group	CH_2	CH	CH_2	CH_2	CH_2	CH_2	CH_2	CH_3	CH_3	CH_3
^{2}H Numbering	3_{ex}	4	5_{ex}	3_{en}	6_{ex}	5_{en}	6_{en}	9	10	8
$\delta(^{1}H)$ [b]	2.25	2.04	1.93	1.74	1.62	1.38	1.34	0.96	0.88	0.84
$\delta(^{1}H)$ (*DMF-d_7*) [c]	2.45	2.21	2.07	1.95	1.83	1.49	1.43	1.08	0.97	0.93
$\delta(^{2}H)$ (*PCBLL/DMF*) [d]	**2.40**	**2.15**	**2.00**	**1.89**	**1.78**	**1.43**	**1.39**	**1.04**	**0.94**	**0.89**
^{13}C Numbering	3	4	5	3	6	5	6	9	10	8
$\delta(^{13}C)$ [e]	43.2	43.0	27.0	43.2	29.8	29.8	27.0	19.1	9.2	19.7
$\delta(^{13}C)$ (*DMF-d_7*) [f]	43.0	43.3	27.0	43.0	30.0	27.0	30.0	18.9	9.2	19.5
$\delta(^{13}C)$ (*PCBLL/DMF*) [g]	42.1	42.3	26.1	42.1	29.1	26.1	29.1	18.0	8.3	18.6
$^{1}J_{CH}$ (*DMF-d_7*) [h]	+129.9	+142.2	+130.9	+132.8	+133.2	+134.1	+133.2	+124.9	+126.0	+124.9
$^{1}T_{CH}$ (*D*) [i]	≈ +164	≈ +157	≈ +89	≈ +114	+146	≈ +120	≈ 102	≈+134	≈ +119	≈ +121
$^{1}T_{CH}$ (*L*) [i]	≈ +136	≈ +140	≈ +89	≈ +124	≈ +124	≈ +120	≈ +84	≈+134	≈ +112	≈ +126
$^{1}D_{CH}$ $^{Exptl.}$ (*D*) [j]	≈ +17	≈ +8	**≈ -21**	**≈ -9**	≈ +7	**≈ -7**	≈ -16	≈+5	≈ -4	≈ -2
$^{1}D_{CH}$ (*L*) [j]	≈ +3	≈ -1	**≈ -21**	**≈ -8**	**≈ -4**	**≈ -7**	**≈ -25**	**≈ +5**	**-7**	≈ +1
$^{1}D_{CH}$ (*average*)	≈ +10	≈ +4	**≈ -21**	**≈ -5**	**≈ +2**	**≈ -7**	**-≈ -21**	**≈ +5**	**≈ -4**	≈ -1
Sign of $^{1}D_{CH}$ $^{Exptl.}$ (*D*)	> 0	> 0	< 0	< 0	> 0	< 0	< 0	> 0	< 0	< 0
Sign of $^{1}D_{CH}$ (*L*)	> 0	< 0	< 0	< 0	< 0	< 0	< 0	> 0	< 0	> 0
Sign of $\Delta\nu_Q(^{2}H)^{Exptl.}$ (*D*)	< 0	< 0	> 0	> 0	< 0	> 0	> 0	< 0	> 0	> 0
Sign of $\Delta\nu_Q(^{2}H)$ (*L*)	< 0	> 0	> 0	> 0	> 0	> 0	> 0	< 0	> 0	< 0
$\Delta\nu_Q^{Exptl.}$ (*D*) [k]	**-221 ± 1**	**+90 ± 1**	**+237 ± 1**	**+115 ± 1**	**-74 ± 1**	**+114 ± 1**	**+199 ± 1**	**-62 ± 1**	**+39 ± 1**	**+28 ± 1**
$\Delta\nu_Q^{Exptl.}$ (*L*) [k]	**+32 ± 1**	**+15 ± 1**	**+162 ± 1**	**-53 ± 1**	**+34 ± 1**	**-62 ± 1**	**+253 ± 1**	**-56 ± 1**	**+81 ± 1**	**+5 ± 1**
$^{1}D_{CH}^{Estim.}$ (*D*) [l]	+19	+8	-21	-10	+7	-10	-17	+5	-3	-3
$^{1}D_{CH}^{Estim.}$ (*L*) [l]	+3	-1	-14	-5	-3	-5	-22	+5	-7	< 1

[a] NMR data ranked from the most deshielded ^{2}H site (Pos. 10) to the most shielded one (Pos. 1) (see the associated tilted NAD 2D spectrum). [b] Data (in ppm) from Kaiser's article (*Magn. Reson. Chem., 1994, (32), 503*). [c] The $\delta(^{1}H)^{iso}$ values (in ppm) experimentally measured in the DMF-d_7 solvent with δ(DMF(CH_3)) = 2.88 ppm. [d] The $\delta(^{2}H)^{aniso}$ values (in ppm) experimentally measured in the **PCBLL** phase (tilted NAD-{^{1}H} *Q*-resolved Fz 2D map) with δ(DMF(CH_3)) = 2.88 ppm (the most shielded CH_3). [e] Data (in ppm) from Crull's article (*Magn. Reson. Chem., 1986, (24), 737).* [f] $\delta\square^{13}C)^{iso}$ (in ppm) experimentally measured in DMF-d_7 with δ(DMF(CH_3)) = 29.76 ppm (the most shielded methyl group). The relative position of ^{13}C peaks for C-3 and C-4 sites are inverted. [g] $\delta(^{13}C)^{aniso}$ values (in ppm) measured in **PCBLL** with δ(DMF(CH_3)) = 29.76 ppm (the most shielded CH_3). [h] $^{1}J_{CH}$ values extracted from the ^{13}C 1D spectrum in DMF-d_7. [i] Approximate $^{1}T_{CH}$ values evaluated from anisotropic ^{13}C-^{1}H spectra (1D and/or 2D T_{CH}-resolved experiments). [j] $^{1}D_{CH}$ (Hz) = [$^{1}T_{CH}$ - $^{1}J_{CH}$]/2. [k] Experimental ^{2}H-RQC values (in Hz) extracted from anisotropic NAD-{^{1}H} *Q*-resolved Fz 2D spectrum. [l] Calculated $^{1}D_{CH}$ values (in Hz) using the relationship: $^{1}D_{CH}^{Estimated} \approx -\Delta\nu_Q^{Exptl}/11.5$.

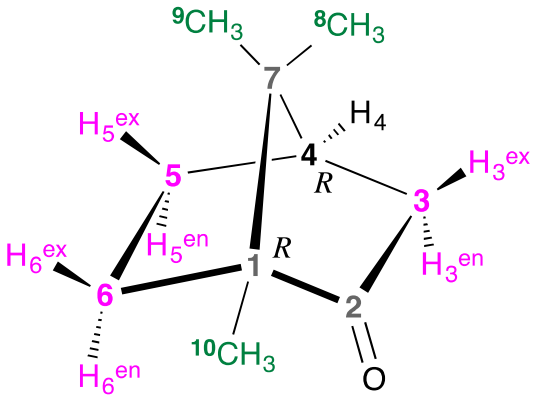

D-camphor (**(*D*)-5**)

Table SI-12. Comparison between ^{2}H-RQC^{Exptl} and ^{2}H-RQC^{Calc} of (*D*) -and (*L*)-**5** dissolved in **PCBLL** => Q(*D*) value = 0.019367 / Q(*L*) value = 0.024128

^{2}H Spect. position [a]	**10**	**9**	**8**	**7**	**6**	**5**	**4**	**3**	**2**	**1**
Group	CH_2	CH	CH_2	CH_2	CH_2	CH_2	CH_2	CH_3	CH_3	CH_3
^{2}H Numbering	**3_{ex}**	**4**	**5_{ex}**	**3_{en}**	**6_{ex}**	**5_{en}**	**6_{en}**	**9**	**10**	**8**
$\Delta\nu_Q^{Exptl.}$ (*D*) / Hz [b]	**-221 ± 1**	**-90 ± 1**	**+237 ± 1**	**+115 ± 1**	**-74 ± 1**	**+114 ± 1**	**+199 ± 1**	**-62 ± 1**	**+39 ± 1**	**+28 ± 1**
$\Delta\nu_Q^{Calc.}$ (*D*) / Hz [c]	**-224.2**	**-92.4**	**233.6**	**115.9**	**-73.8**	**109.4**	**198.9**	**-63.0**	**43.4**	**29.4**
$\Delta\Delta\nu_Q$ / Hz [d]	-3.2	-2.4	-3.4	0.9	0.2	-4.6	-0.2	-1.0	4.4	1.4
Rel. D□□□. (%) [e]	1.4	2.6	1.4	0.8	0.3	4.2	0.1	1.6	10.1	4.6
$\Delta\nu_Q^{Exptl.}$ (*L*) / Hz [b]	**+32 ± 1**	**+15 ± 1**	**+162 ± 1**	**-53 ± 1**	**+34 ± 1**	**-62 ± 1**	**+253 ± 1**	**-56 ± 1**	**+81 ± 1**	**+5 ± 1**
$\Delta\nu_Q^{Calc.}$ (*L*) / Hz [c]	**29.0**	**11.8**	**158.8**	**-52.4**	**+34.4**	**-66.8**	**+253.6**	**-55.4**	**+83.4**	**+7.0**
$\Delta\Delta\nu_Q$ / Hz [d]	-3.1	-3.2	-3.2	+0.6	+0.4	-4.8	+0.6	+0.6	+2.4	+2.0
Rel. D□□□. (%) [e]	10.5	27.4	2.0	1.1	1.0	7.1	0.2	1.0	2.9	28.3

[a] ^{2}H NMR data ranked from the most deshielded ^{2}H site (Pos. 10) to the most shielded one (Pos. 1) (see the associated tilted NAD 2D spectrum. [b] Experimental ^{2}H-RQC values extracted from ANAD-{^{1}H} *Q*-resolved-Fz 2D spectrum. [c] Back-calculated ^{2}H-RQCs calculated (best SVD-fit) using ConArch$^+$ program. [d] $\Delta\Delta\nu_Q = \Delta\nu_Q^{Calc.}(D) - \Delta\nu_Q^{Exptl.}(D)$. [e] Relative difference: Rel. Diff. (%) = $|\Delta\nu_Q^{Calc.}(D) - \Delta\nu_Q^{Exptl.}(D)| / |\Delta\nu_Q^{Calc.}(D)|$.

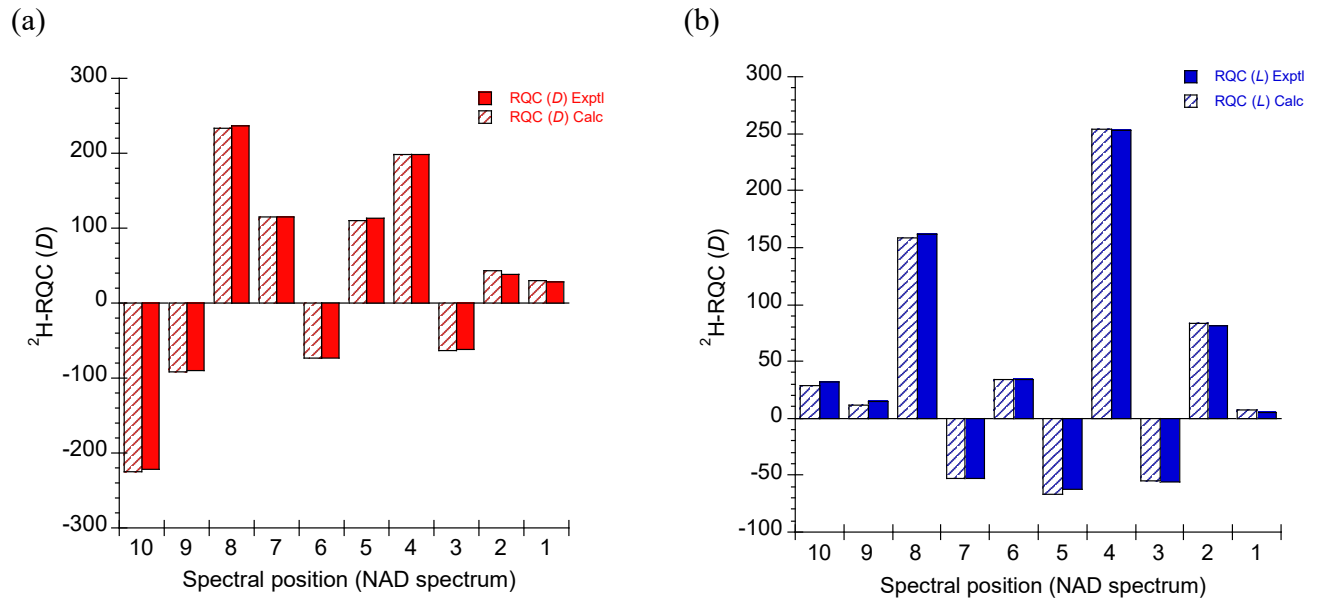

Figure SI-25. Comparison between ^{2}H-RQC$^{\text{Exptl.}}$ and ^{2}H-RQC$^{\text{Calc.}}$ values *versus* the position ^{2}H-DQs on the NAD F_2 projection of the *Q*-resolved map of **5** (see **Figure SI-15**) dissolved in the PCBLL mesophase: (a) (*L*)-enantiomer, (b) (*D*)-enantiomer.

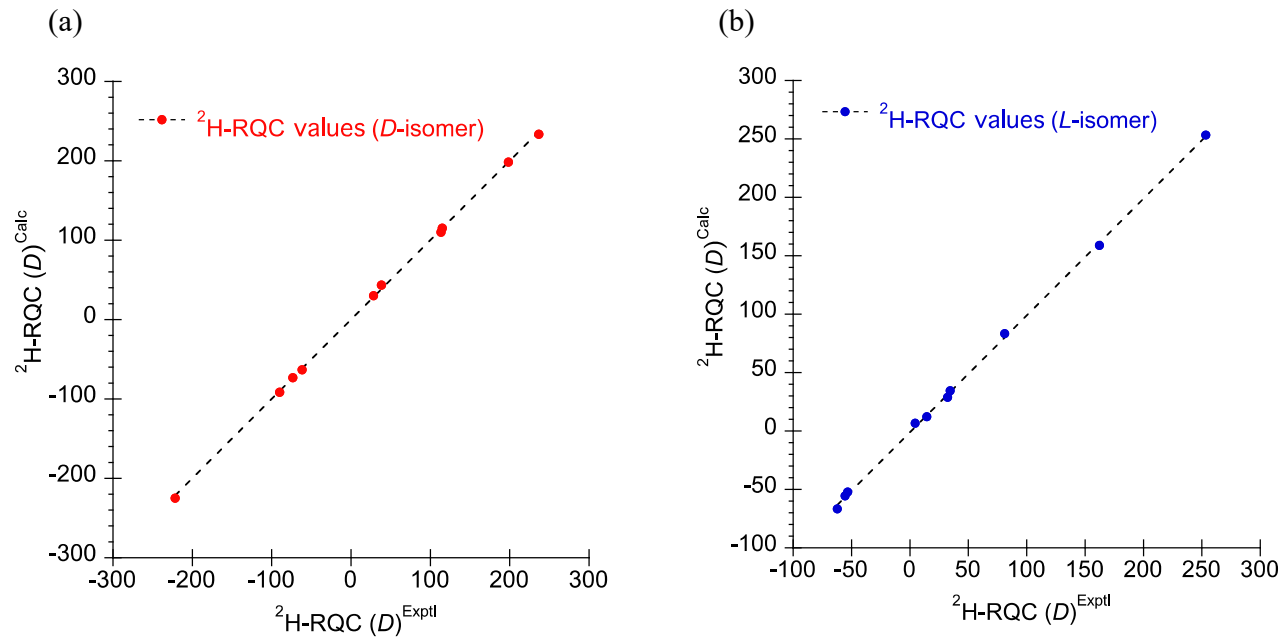

Figure SI-26. Correlation plots (^{2}H-RQC$^{\text{Calc.}}$ *versus* ^{2}H-RQC$^{\text{Exptl.}}$) of **5** dissolved in the PCBLL mesophase obtained for the best-fit data/structure: (a) (*D*-enantiomer, (b) (*L*)-enantiomer. The *Q*-factor obtained is equal to 0.0194 and 0.0241, respectively.

XV. Output correlation plots for each chiral mesophase

Below are the experimental *versus* back-calculated correlation plots (red line) as well as the confidence and prediction intervals (unweighted) provided by the ConArch^{+} program for each enantiomer and the four chiral mesophases.

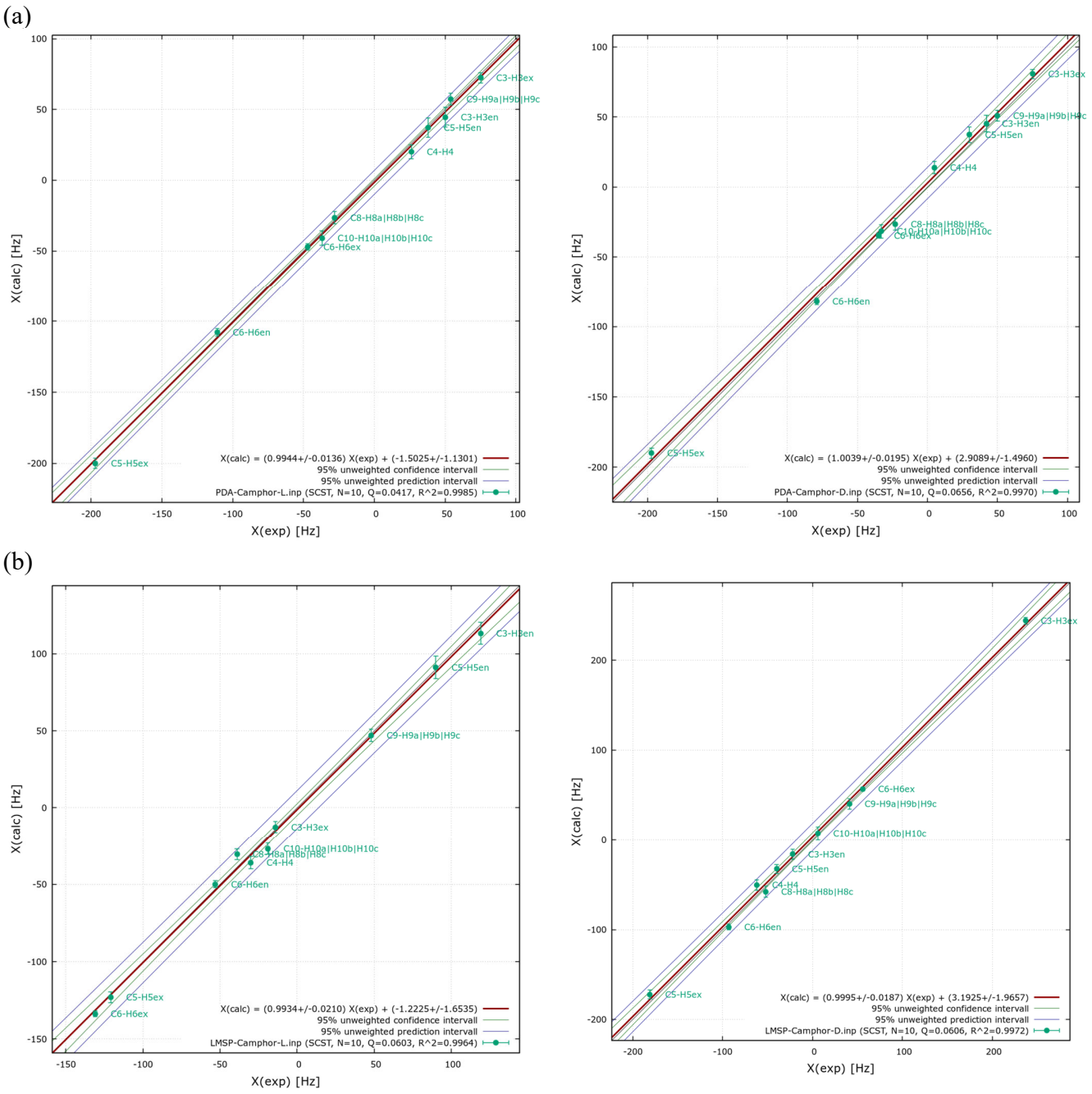

Figure SI-27. Output correlation plots (^{2}H-RQC$^{Calc.}$ *versus* ^{2}H-RQC$^{Exptl.}$) of **5** dissolved in (a) PDA and (b) L-MSP mesophases for the (*L*)- and (*D*)-enantiomer (left and right panel, respectively) displayed with the ConArch^{+} program.

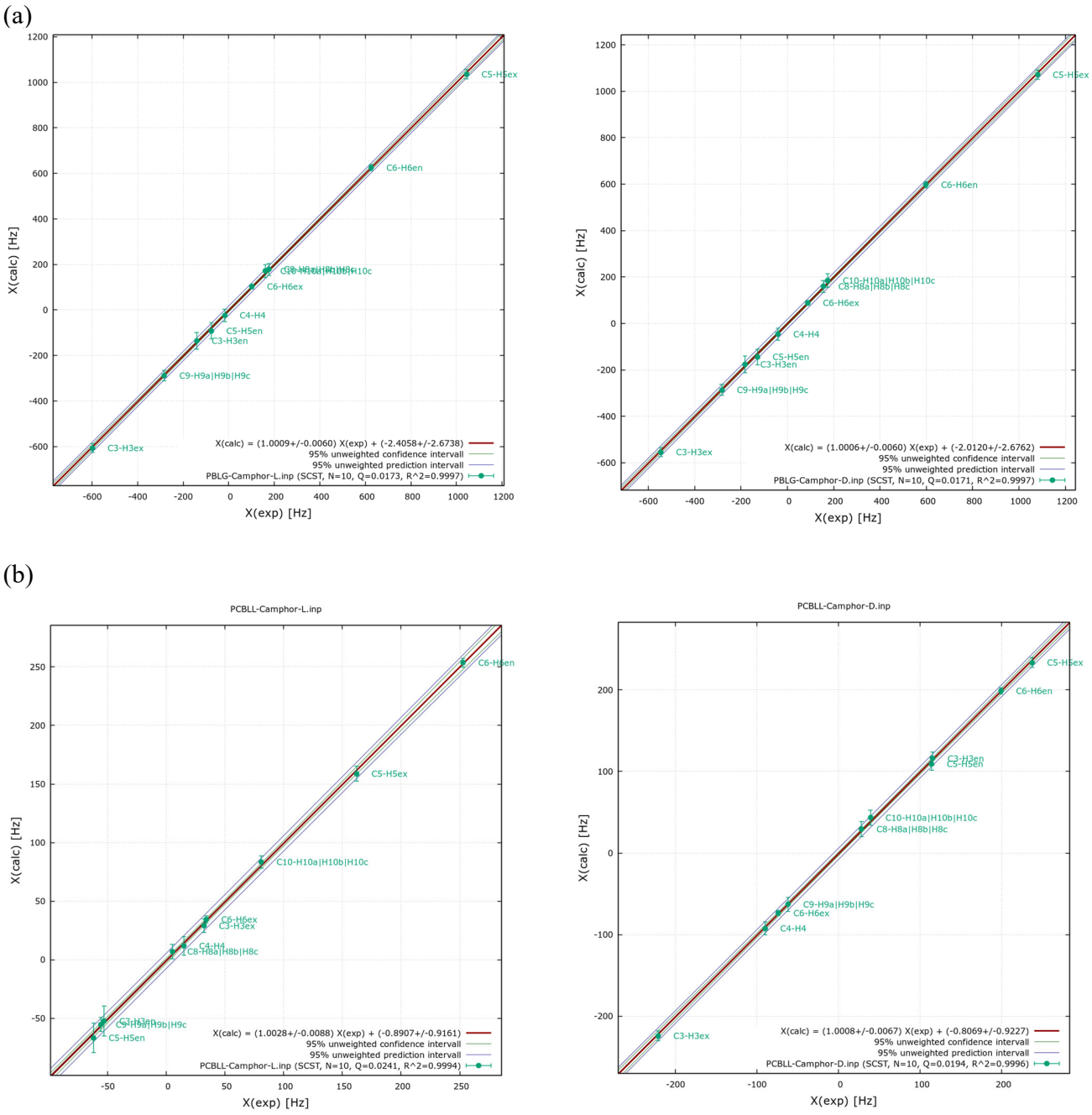

Figure SI-28. Output correlation plots (^{2}H-RQC$^{\text{Calc.}}$ *versus* ^{2}H-RQC$^{\text{Exptl.}}$) of **5** dissolved in (a) PBLG and (b) PCBLL mesophases for the (*L*)- and (*D*)-enantiomer (left and right panel, respectively) displayed with the ConArch+ program.

XVI. References for Supporting Information

[**1**] P. Lesot, P. Berdagué, A. Meddour, A. Kreiter, M. Noll and M. Reggelin. ^{2}H and ^{13}C NMR-based Enantiodetection using Polyacetylene *versus* Polypeptide Aligning Media: Versatile and Complementary Tools for Chemists, *ChemPlusChem.* 2019, **84**, 144-153.

[**2**] A. Meddour, D. Atkinson, A. Loewenstein and J. Courtieu, Enantiomeric Analysis of Homologous Series of Secondary Alcohols by Deuterium NMR Spectroscopy in a Chiral Nematic Liquid Crystal: Influence of Molecular Geometry on Chiral Discrimination, *Chem. Eur. J.* 1998, **4**, 1142-1147.

[3] J. Courtieu, C. Aroulanda, P. Lesot, A. Meddour and D Merlet, Evolution of the Saupe Order Parameters of Enantiomers from a Non-chiral to a Chiral Liquid Crystal Solvent: an Original Light on the Absolute Configuration Problem, *Liq. Crystals,* 2010, **7**, 903-912.

[4] P. Lesot, Z. Serhan, C. Aroulanda and I. Billault, Analytical Contribution of NAD 2D-NMR Spectroscopy in Polypeptide Mesophases to the Investigation of Triglycerides, *Magn. Reson. in Chem.* 2012, **50**, S2-S12.

[**5**] C. Aroulanda, D. Merlet, J. Courtieu and P. Lesot, NMR Experimental Evidence of the Differentiation of Enantiotopic Directions in C_s and C_{2v} Molecules using Partially Oriented, Chiral Media, *J. Am. Chem. Soc*. 2001, **123**, 12059-12066.

[**6**] P. Lesot, C. Aroulanda, H. Zimmermann and Z. Luz, Enantiotopic Discrimination in the NMR Spectrum of Prochiral Solutes in Chiral Liquid Crystals, *Chem. Soc. Rev*. 2015, **44**, 230-275.

[**7**] P. Lesot, C. Aroulanda, P. Berdagué, A. Meddour, D. Merlet, J. Farjon, N. Giraud and O. Lafon, Multinuclear NMR in Polypeptide Liquid Crystals: Three Fertile Decades of Methodological Developments and Analytical Challenges, *Prog. Nucl. Magn. Reson. Spectrosc.* 2020, **116**, 85-154.

[**8**] P. Lesot and O. Lafon, O. Natural Abundance ^{2}H NMR Spectroscopy, in *Encyclopedia of Spectroscopy and Spectrometry*, *Eds.* Lindon, Tranter and Kopenaal, Elsevier / Academic Press, 2017, 3rd Ed., Vol. 3, pp. 1-14.

[**9**] S. Immel, M. Köck and M. Reggelin, Configurational Analysis by Residual Dipolar Coupling Driven Floating Chirality Distance Geometry Calculations, *Chem. Eur. J.* 2018, **24**, 13918-13930.

[**10**] G. Cornilescu and A. Bax, Measurement of Proton, Nitrogen, and Carbonyl Chemical Shielding Anisotropies in a Protein Dissolved in a Dilute Liquid-crystalline Phase, *J. Am. Chem. Soc.* 2000, **122**, 10143-10154.

[**11**] J.R., Tolman, H.M Al-Hashimi, E. Kay and J.H. Prestegard, Structural and Dynamic Analysis of Residual Dipolar Coupling Data for Proteins, *J. Am. Chem. Soc*. 2001, **123**, 1416-1424.

[**12**] F. Kramer, M.V. Deshmukh, H. Kessler and S.J Glaser,.Residual dipolar coupling constants: An elementary derivation of key equations, *Concepts Magn. Reson*. 2004, **21A**, 10-21.

[13] H.E. Gottlieb, V. Kotlyar and A. Nudelman, NMR Chemical Shifts of Common Laboratory Solvents as Trace Impurities, *J. Org. Chem*. 1997, **62***,* 7512-7515.

[**14**] Y. Koseki, H. Yamada, T. Usuki, Efficient Synthesis of Benzyl 2-(*S*)-[(tert-butoxycarbonyl) amino]-ω-iodoalkanoates, *Tetrahedron: Asymmetry*, 2011, **22**, 580-586.

[15] E. Yashima, T. Matsushima and Y. Okamoto, Chirality Assignment of Amines and Amino Alcohols Based on Circular Dichroism Induced by Helix Formation of a Stereoregular Poly((4carboxyphenyl) acety-lene) through Acid−Base Complexation, *J. Am. Chem. Soc.* 1997, **119**, 6345-6359.

[16] X.S. Ma, H. Dang, J.A. Rose, P. Rablen and S.B. Herzon, Hydroheteroarylation of Unactivated Alkenes using N-Methoxyheteroarenium Salts, *J. Am. Chem. Soc.* 2017, **139**, 5998-6007.

[**17**] Y. Misumi and T. Masuda, Living Polymerization of Phenylacetylene by Novel Rhodium Catalysts. Quantitative Initiation and Introduction of Functional Groups at the Initiating Chain End, *Macromolecules,* 1998, **31**, 7572-7573.